Novel Staphylococcal Inhibitors of Neutrophil Granule Enzymes

by

Nicoleta Teodora Ploscariu

B.S., Alexandru Ioan Cuza University, 2009
M.S., Alexandru Ioan Cuza University, 2011
M.S., Kansas State University, 2014

AN ABSTRACT OF A DISSERTATION

submitted in partial fulfillment of the requirements for the degree

DOCTOR OF PHILOSOPHY

Department of Biochemistry and Molecular Biophysics
College of Arts and Sciences

KANSAS STATE UNIVERSITY
Manhattan, Kansas

2018

Abstract

Neutrophils are our most abundant white blood cells and the first leukocytes to infiltrate sites of infection or damaged/healing tissue. Activation of neutrophils results in the mobilization of several types of granules stored within their cytosol, such as the so-called azurophilic granules, which either fuse with the maturing endophagocytic compartment or are released into the extracellular environment. One of the most abundant component of azurophilic granules is a heme-containing enzyme called myeloperoxidase (MPO), which reduces the H_2O_2 produced by the neutrophil's respiratory burst to generate cytotoxic hypohalous acids, most typically HOCl. While neutrophil granule enzymes are essential for our innate defenses, neutrophil-driven inflammation outside this beneficial context lies at the heart of many non-infectious human diseases.

Staphylococcus aureus and closely related species are highly adapted to their hosts and have evolved many strategies to resist opsonization and phagocytosis. *S. aureus* shows resistance to killing following uptake into the phagosome, which suggests that the bacterium can actively evade specific intracellular killing mechanisms used by neutrophils. Recent work found a highly conserved *S. aureus* protein, SPIN (for Staphylococcal Peroxidase INhibitor), that specifically binds and inhibits MPO [1].

This study was focused on characterizing the structure/function relationship for MPO inhibitors, SPIN proteins. To identify key residues for SPIN function in more detail, we examined two types of SPIN proteins using structural methods, direct binding assays, and functional assays for MPO activity: deletion mutants and SPIN proteins originating from divergent staphylococcal species.

Together, these studies shed light on the molecular features which determine the specificity of SPIN proteins for MPO and suggest potential avenues for using this information toward the design of synthetic MPO inhibitors. In addition to the focus on targeted inhibition of MPO for its therapeutic value in treatment of a number of significant human inflammatory diseases, our investigations contributed in expanding our knowledge on infection spreading. As a first cellular host defense response, the neutrophil interaction with pathogens are of major interest. Characterization of staphylococcal immune evasion proteins is vital for understanding bacterial survival when encountering neutrophils and their bioactive constituents.

Novel Staphylococcal Inhibitors of Neutrophil Granule Enzymes

by

Nicoleta Teodora Ploscariu

B.S., Alexandru Ioan Cuza University, 2009
M.S., Alexandru Ioan Cuza University, 2011
M.S., Kansas State University, 2014

A DISSERTATION

submitted in partial fulfillment of the requirements for the degree

DOCTOR OF PHILOSOPHY

Department of Biochemistry and Molecular Biophysics
College of Arts and Sciences

KANSAS STATE UNIVERSITY
Manhattan, Kansas

2018

Approved by:

Major Professor
Brian V. Geisbrecht

Copyright

Abstract

Neutrophils are our most abundant white blood cells and the first leukocytes to infiltrate sites of infection or damaged/healing tissue. Activation of neutrophils results in the mobilization of several types of granules stored within their cytosol, such as the so-called azurophilic granules, which either fuse with the maturing endophagocytic compartment or are released into the extracellular environment. One of the most abundant component of azurophilic granules is a heme-containing enzyme called myeloperoxidase (MPO), which reduces the H_2O_2 produced by the neutrophil's respiratory burst to generate cytotoxic hypohalous acids, most typically HOCl. While neutrophil granule enzymes are essential for our innate defenses, neutrophil-driven inflammation outside this beneficial context lies at the heart of many non-infectious human diseases.

Staphylococcus aureus and closely related species are highly adapted to their hosts and have evolved many strategies to resist opsonization and phagocytosis. *S. aureus* shows resistance to killing following uptake into the phagosome, which suggests that the bacterium can actively evade specific intracellular killing mechanisms used by neutrophils. Recent work found a highly conserved *S. aureus* protein, SPIN (for Staphylococcal Peroxidase INhibitor), that specifically binds and inhibits MPO [1].

This study was focused on characterizing the structure/function relationship for MPO inhibitors, SPIN proteins. To identify key residues for SPIN function in more detail, we examined two types of SPIN proteins using structural methods, direct binding assays, and functional assays for MPO activity: deletion mutants and SPIN proteins originating from divergent staphylococcal species.

Together, these studies shed light on the molecular features which determine the specificity of SPIN proteins for MPO and suggest potential avenues for using this information toward the design of synthetic MPO inhibitors. In addition to the focus on targeted inhibition of MPO for its therapeutic value in treatment of a number of significant human inflammatory diseases, our investigations contributed in expanding our knowledge on infection spreading. As a first cellular host defense response, the neutrophil interaction with pathogens are of major interest. Characterization of staphylococcal immune evasion proteins is vital for understanding bacterial survival when encountering neutrophils and their bioactive constituents.

Table of Contents

List of Figures

List of Tables

Chapter 1 - Introduction

While humans have gone to great lengths to understand our inflammatory systems and the impact they have on our health, successful pathogens must confront and evade these very same systems to survive inside our body. Numerous studies have demonstrated that the bacterial pathogen *Staphylococcus aureus* deploys an array of evolutionarily-optimized innate immune evasion proteins, some of which effectively block key events within our inflammatory system [2-4]. One of the first host defense components that the invading pathogens encounter are the neutrophils. Therefore, it is a great selective pressure for bacteria to develop mechanism that allows it to effectively bypass, subvert, or disrupt neutrophil function.

The work presented in this manuscript is focused towards characterizing a novel protein of staphylococcal origin, SPIN (for Staphylococcal Peroxidase INhibitor), that specifically binds and inhibits a neutrophil enzyme which is essential for bacterial killing [1]. Through a multi-disciplinary collaboration, it was shown that SPIN is required for maximal S. *aureus* virulence in animal infection models. Also, *S. aureus* cells deleted for SPIN gene showed decreased survival compared to wild-type bacteria after phagocytosis by neutrophils. In the same study, a crystal structure of SPIN-*aureus* bound to recombinant human MPO suggests that the inhibitor is using its N-terminus as a molecular plug to prevent H_2O_2 substrate access to the MPO active site.

Here, a detailed analysis of the structure/function and mechanism of this novel class of inhibitors is provided. The purpose of this work is to expand our understanding of the neutrophil's enzymatic components, such as MPO, which may provide unique information to guide design of anti-inflammatory and anti-bacterial therapies.

1.1 Neutrophils role in human innate immune system

Neutrophils are the most abundant white blood cells in human circulation and key players in the first line defense against invading bacteria [3, 4]. Upon activation, neutrophils phagocytose pathogens whereby their various intracellular granules fuse with the maturing phagosome [5, 6]. Efficient phagocytic killing is a complex process dependent upon the various antimicrobial proteins and peptides contained within neutrophils' subcellular granules (Reviewed in [3-7]).

The most abundant component of azurophilic granules is the enzyme myeloperoxidase (MPO). In the presence of halides, MPO converts hydrogen peroxide (H_2O_2) into bactericidal hypohalous acids, such as HOCl and HOBr [7].

As the phagosomal compartment matures, an enzymatic system that leads to generation of diverse reactive oxidant species assembles within its membrane. Activity of the multipartite NADPH oxidase converts O_2 into $O_2^{-\bullet}$, which dismutates either directly or enzymatically into H_2O_2. Although H_2O_2 on its own is mildly cytotoxic, it also serves as a substrate for the abundant heme-dependent granule enzyme, MPO. MPO generates highly toxic and reactive oxidant species, most notably hypochlorous acid (HOCl). Using a model for the neutrophil phagosome, it was estimated that the concentration of MPO is 1 mM [8].

Neutrophil granules likewise contain high levels of antibacterial peptides and proteases, such as neutrophil elastase (NE), cathepsin G (CG), and proteinase-3 (PR3). While these proteases on their own are sufficient to kill certain bacteria [9-11], there is evidence to suggest that they function synergistically with MPO-derived oxidants to enhance killing of bacteria trapped within the phagosome [12]. Thus, the abundant and overlapping anti-bacterial systems acting within the neutrophils' phagosomal compartment present a formidable innate defense against infection.

Azurophilic granules also contain high concentrations of chymotrypsin-like proteases (NSPs), which can directly attack certain bacterial cells and/or the secreted and surface-retained proteins these cells produce [9-11]. Although the activities of MPO and NSPs are typically viewed as independent entities, some studies have indicated that these two systems have synergistic effects with one another inside the phagosome [13]. Thus, the concerted action of MPO and NSPs forms a foundation of neutrophil-mediated defense against potentially infectious bacteria.

1.2 *Staphylococcus aureus* immune evasion strategies of neutrophils

The pathogenic bacterium *S. aureus* is a rising threat to human health and is known for its ability to cause a large range of infections, affecting from skin and soft tissues to bone and joints as well as leading to respiratory and endovascular disorders. While most of these infections can be resolved, there are several manifestations that can lead to life-threatening infections, such as bacteremia, endocarditis, sepsis and toxic shock syndrome [2, 14]. *S. aureus* has also a tendency to spread and cause recurrent infections at different sites, known as metastatic infections [15, 16].

Invading pathogens are subjected to a nearly instantaneous assault by their host's innate immune system. As a consequence, there is heavy selective pressure for these organisms to evolve the molecular wherewithal that provides for escape from the innate immune response. While extensive study of various pathogens has cataloged an array of these so-called immune evasion strategies, the Gram-positive bacterium *S. aureus* appears to be particularly adept at

attempting to block the events that lead to its opsonization with complement components and subsequent phagocytosis by neutrophils [2, 17-19].

To circumvent the interaction with neutrophils, *S. aureus* secretes an array of proteins that can prevent their migration to the site of infection. As such, superantigen-like proteins (SSLs) [20-22]can interfere with the neutrophil adhesion/rolling process, while other classes of proteins are interfering with the physiological functions of immune cells, phenol-soluble modulins (PSMs) [23]or counter the neutrophil chemotaxis, chemotaxis inhibitory protein of *S. aureus* (CHIPS) [24] and formyl peptide receptor-like 1 inhibitor (FLIPr and FLIPr-L) [2, 25].

Recent work has shown that a portion of those *S. aureus* cells that undergo phagocytosis survive, leading to speculation that these leukocytes might serve as "Trojan Horses" for bacterial dissemination in vivo [15]. For this to be the case, we believe that *S. aureus* is likely engaged in an elaborate immune evasion program that acts intracellularly, and likely within the maturing phagosome. Indeed, our discovery of *S. aureus* extracellular adherence proteins (EAPs) as highly selective NSP inhibitors that promote virulence is consistent with this hypothesis [26]. Other strategies to survive such toxic environment that have been previously characterized involve resistance to lysozyme and antimicrobial peptides which can be blocked by lysyl- or alanyl-phosphatidylglycerol synthesis (MprF) and peptidoglycan acetylation (OatA), and staphylococcal pigments (staphyloxanthin), catalase (KatG), alkylhydroperoxyde reductase (AhpC) and superoxide dismutases (SodA, SodM) offer protection against hydrogen peroxide, hydroxyl radicals and neutrophil superoxide [2, 27-31].

Using a recently deployed a phage display strategy, secreted *S. aureus* proteins that interact with putative evasion targets found within neutrophils were identified [32]. Since MPO

is the most abundant component of azurophilic granules [7, 33], it represented a promising initial candidate for this approach.

A novel protein, of 8.4 kDa, named SPIN for Staphylococcal Peroxidase Inhibitor was found to bind and inhibit human MPO [1]. Gene expression studies revealed that *spn* transcription is upregulated following phagocytosis of *S. aureus* cells by neutrophils, suggesting that the SPIN protein operates primarily within the phagosomal compartment [1]. Through subsequent studies, it was found that SPIN protects *S. aureus* from MPO-mediated killing and thereby established SPIN as a novel immune evasion protein of *S. aureus* [1].

SPIN shows no sequence similarity to other characterized proteins, which initially prevented understanding of its effects on MPO. To circumvent this limitation, a 2.4 Å resolution crystal structure of SPIN bound to a recombinant form of human MPO (i.e. rMPO) was solved [1]. This structure suggested that SPIN acts by occluding the exchange of substrate, product, and bulk solvent with the reactive heme that lies the within the MPO active site.

While a majority of the SPIN protein adopts a three α-helical bundle fold, inspection of the crystal structure suggested that this helical bundle might not be responsible *per se* for inhibiting MPO. Instead, an approximately 10-residue extension at the SPIN N-terminus assumes a β-hairpin structure which almost completely occupies the MPO active site channel [1].

Further examination of the SPIN structure suggested that this N-terminal β-hairpin might not be intrinsically stable in the absence of its MPO ligand, however, as it lacks features such as disulfide bonds, etc., that would constrain these two short β-strands into their MPO-bound conformation.

1.3 Summary

Although decades of research enabled our understanding human inflammatory pathways and their impact on our health, the experts in understanding and evading these systems are in fact our most successful pathogens. The bacterial pathogen *S. aureus,* has developed an array of evolutionary-optimized proteins which allows its survival by evading and blocking key events within our inflammatory system.

The work in this dissertation is focused towards characterizing the structure/function relationship of one class of proteins of staphylococcal origin, SPIN. SPIN protein originating from *S. aureus* has been found to inhibit the activity of human MPO and therefore, has a great potential to serve as a template for the design of anti-inflammatory and anti-bacterial therapies.

In the first part of this study, as presented in Chapter 3, we characterized the structure of SPIN in both free and bound form using both x-ray crystallography and solution NMR. In the following parts of the study, Chapters 4 and 5, we have complemented the structural studies with biochemical and functional analyses of the MPO-SPIN interaction.

In addition to the focus on targeted inhibition of MPO for its therapeutic value in treatment of a number of significant human inflammatory diseases, our investigations have been aimed towards expanding our knowledge on infection spreading. Since neutrophils are the first cell-mediated host defense, their interaction with pathogens are of major interest. Characterization of staphylococcal immune evasion proteins is vital for understanding bacterial survival when encountering neutrophils and their bioactive constituents.

Chapter 2 - Methodology

This Chapter contains the details of the materials and methods used for this study. The first section provides the cloning technique and purification strategy to obtain the SPIN proteins and the site-directed mutants. The next sections are describing different experimental techniques that have been used to characterize the proteins, both biochemically and structurally. Some protocols used for functional determination have been provided, as published for the papers under Chapters 4 and 5, although they contain the work of our collaborators.

2.1 Protein Preparation

2.1.1 Recombinant Protein Expression and Purification

The sequences of the predicted mature form (lacks the N-terminal signal sequence) of various SPIN homologs were codon optimized for *E. coli* expression using the Sequence Manipulation Suite Reverse Translate tool (http://www.bioinformatics.org/sms2/rev_trans.html) [34]. The corresponding DNA fragments were synthesized as gBlocks Gene Fragments (Integrated DNA Technologies; Coralville, IA, USA) with *Bam*H1 and *Not*1 sites appended at the 5' and 3' ends, respectively. The only exception was the *S. aureus* SPIN, for which the sequence was synthesized with *SalI* and *EcoRI* sites.

Each of the coding fragments were subcloned into the *Bam*HI and *Not*1 (*SalI* and *EcoRI* for SPIN-*aureus*) sites of a modified form of the prokaryotic expression vector pT7HMT [35]. All other expression vectors for site-directed mutants of SPIN-*aureus* were derived from this parental plasmid and were constructed using standard mutagenic PCR approaches.

The integrity of each insert was verified by DNA sequencing prior to transformation into *E. coli* BL21(DE3) cells for protein expression as previously described [1, 35, 36]. Briefly, recombinant strains of E. coli BL21(DE3) bearing a plasmid of interest were grown in 1 L of selective Terrific Broth at 37 ºC. When the OD at 600 nm reaches 0.6, the protein expression was induced with 1 mM IPTG at 18 ºC overnight. Cells from the induced culture were harvested by centrifugation, resuspended, lysed by microfluidization, and processed for chromatography purification [37].

The vector pT7HMT encodes an N-terminal 6-His affinity tag that is used for Ni^{2+}affinity chromatography purification of the protein, but which can be removed by digestion with Tobacco Etch Virus (TEV) protease [35]. Following TEV cleavage, the recombinant form of each SPIN protein contains an artificial “GSTGS” (“GST” for SPIN-*aureus*) amino acid sequence at its N-terminus. Analogous residues arising from the subcloning procedure are not visible in the co-crystal structure of SPIN-*aureus* bound to human MPO [36], and thus are not believed to influence the physical nature of the SPIN/MPO complex.

Following initial purification, the recombinant SPIN proteins were digested with TEV protease to remove the affinity tag, followed by a reverse Ni^{2+}affinity chromatography, where the flow through contains the untagged protein. Final purification was achieved by gel-filtration chromatography in a buffer of PBS (pH 7.4) using a Superdex 75 26/60 column connected to an AKTA FPLC system (GE Life Sciences).

All SPIN proteins were analyzed by MALDI-TOF mass spectrometry for both purity and integrity prior to their usage in subsequent experiments.

2.1.2 Protein Expression and Purification for NMR

Uniformly ^{15}N and $^{15}N/^{13}C$ double-labeled SPIN proteins were prepared for NMR spectroscopy studies. Both forms of wild-type SPIN were expressed in *E.coli* BL21(DE3) cells grown in minimal medium (M9) enriched with $^{15}NH_4Cl$ and ^{13}C-glucose as described before [38].

The purified protein yield from 1 L of *E. coli* culture was in the range of 7-9 mg for both ^{15}N and $^{13}C/^{15}N$ double-labeled SPIN. The samples for NMR experiments contained 0.75 - 1.0 mM uniformly ^{15}N or $^{13}C/^{15}N$ double-labeled SPIN protein in 50 mM sodium phosphate buffer (pH 6.5) containing 5 % (v/v) D_2O (used as a lock solvent).

2.1.3 Synthetic Peptide Mimics of the SPIN N-terminus

This section has been reproduced in this current format from de Jong et al., Copyright © 2018, The American Society for Biochemistry and Molecular Biology, Inc.

Peptides SKVYSQNGLVLHDDS (i.e. SPIN-p1) and CKVYSQNGLVLHDDC (i.e. SPIN-p2) were synthesized at >90% purity by GenScript (Piscataway, NJ). Peptide SPIN-p2 was chemically oxidized to form a disulfide bond between its two cysteine residues. The identity of each product was confirmed by MALDI-TOF prior to use. Peptide stock solutions were prepared at 5 mM in ddH_2O.

2.1.4 Human Neutrophil Protein Preparations

This section has been reproduced in this current format from de Jong et al., Copyright © 2018, The American Society for Biochemistry and Molecular Biology, Inc.

Two different forms of human myeloperoxidase were used during the course of this work. Native human myeloperoxidase (MPO) that had been chromatographically isolated from purulent sputum was obtained from Elastin Products Corp. (Owensville, MO; catalog # MY862) and was used for biochemical and functional analyses. A recombinant form of human MPO (rhMPO) bearing a C-terminal 10-His tag was purchased from R&D Systems (Minneapolis, MN; catalog # 3174-MP-250) and was used for structural studies.

The neutrophil serine proteinases Neutrophil Elastase (catalog #SE563), Cathepsin G (catalog #SG623), and Proteinase-3 (catalog #ML734) were likewise isolated from purulent human sputum and obtained from Elastin Products Corp. (Owensville, MO).

All materials were in lyophilized form which we reconstituted and handled as suggested by the supplier unless otherwise noted.

2.2 Surface Plasmon Resonance Binding Affinity Determination

Direct binding studies of SPIN proteins to native human MPO were performed on a Biacore T-200 instrument (GE Healthcare) [1]. All experiments were carried at 25 ºC using a running buffer of 20 mM HEPES (pH 7.4), 140 mM NaCl, and 0.005% (v/v) Tween-20 and a flowrate of 30 µl/min.

Experimental surfaces were created on CMD 200M sensor chips (XanTec Bioanalytics GmbH; Dusselorf, Germany) by coupling native human MPO on three separate flow cells via random amine chemistry. MPO was immobilized at different levels on each flow cell to allow for replicate measurements while ensuring that surface density did not substantially affect the interaction parameters; two flow cells had a relatively high level of MPO at 7155 and 7311 resonance units (RU), respectively, while a third flow cell was derivatized with 2829 RU of MPO. A reference surface was also prepared by activation followed by immediate inactivation with ethanolamine.

A concentration series for each SPIN proteins (0 - 1,000 nM) was injected over the flow cells for 3 min, followed by a 4 min dissociation phase. Regeneration to baseline was achieved by two consecutive 0.5 min injections of 0.1 M glycine (pH 10.0). Data processing was performed using Biacore T-200 Evaluation Software v3.0 (GE Healthcare). Each reference subtracted injection series was analyzed using a 1:1 binding model (Langmuir) and fitting Rmax locally. The fitted binding curves and were imported and graphed in Igor Pro (Wavemetrics) and the resonance units (RU) were normalized to the maximal response for each experimental series.

The ability of SPIN peptides to compete with SPIN/MPO complex formation was assessed using an SPR-based competition assay. The experiments were performed on the same instrument at 25°C using a flowrate of 30 µl min-1 in HBS-T running buffer.

Injections were performed for 1 min and dissociation was monitored for 3 min at which point baseline regeneration was achieved as described above. SPIN (50 nM) or SPIN peptides (50 µM) were injected either alone or as a mixture (i.e. SPIN + peptide) over the MPO surface and the response was monitored. Residual response of SPIN during co-injections was calculated

by subtracting the response of the peptide-only injections. Sensorgram overlays for these experiments were prepared also using Biacore T-200 Evaluation Software and GraphPad Prism.

2.3 Myeloperoxidase Assays

2.3.1 Myeloperoxidase activity assay

This section has been reproduced in this current format from de Jong et al., Copyright © 2018, The American Society for Biochemistry and Molecular Biology, Inc.

To determine the function of the SPIN proteins as MPO inhibitors, we performed a study where we measured spectrophotometrically the redox indicator o-dianisidine (OD at 450 nm) in the presence of MPO substrate (H_2O_2) [1].

MPO activity in the presence of H_2O_2 as a substrate and o-dianisidine as a redox indicator was monitored at 450 nm [1]. Briefly, 0.2 U/mL MPO isolated from human sputum (Elastin Products Company) was incubated with 74 nM of various SPIN proteins for 1 h at 37 °C in 96-well plates to allow protein-protein interactions to form. A study in which the same MPO, 0.2 U/mL was incubated with several dilutions (2000 nM to 1 nM) of SPIN proteins was also carried as presented in Chapter 5. A substrate mixture comprised of 45 mM phosphate buffer (pH 6.0), 0.5 mM H2O2, and 15 μg of o-dianisidine dihydrochloride (Sigma-Aldrich catalog #D9154) was then added.

The OD450 nm was measured continuously every 45 seconds for 1 h at 37 °C using a FLUOstar Omega microplate reader. The slope of each trial before saturation was calculated via

GraphPad Prism 6 and defined as MPO activity. BSA was used as a negative control for inhibition.

The influence of NSPs on MPO inhibition by SPIN was also examined through a similar approach. Specifically, full-length SPIN was pre-incubated for 1 h at 37 °C with either 18 µg/mL NE, 4.5 µg/mL CG, or 4.5 µg/mL PR3 after which 1 mM PMSF was added to stop protease activity. The SPIN digestion reaction was then serially diluted and assayed for MPO activity as described above. Where indicated, NSPs were also pre-incubated for 5 min at room temperature with 37.5 µg/mL Eap prior to adding this mixture to full-length SPIN.

2.3.2 MPO bactericidal assay

This section has been reproduced in this current format from de Jong et al., Copyright © 2018, The American Society for Biochemistry and Molecular Biology, Inc.

S. aureus cells were grown to logarithmic phase (OD660 ~0.5) in Todd Hewitt Broth (THB), washed twice, and resuspended to an OD660 ~0.5 in sterile Hanks Balanced Salt Solution (HBSS). 100 µL of bacterial suspension were diluted into 10 mL of substrate solution containing 300 mM glucose in HBSS. 50 µL of this mixture were diluted with an equal part of enzyme solution containing 4 ng/mL Glucose Oxidase from Aspergillus (Sigma-Aldrich), and 2.3 nM MPO with or without the addition of 40 nM SPIN proteins. The enzyme/bacteria mixture was incubated for 1 hour at 37°C and peroxidase activity was stopped by addition of 10 mg/mL catalase from bovine liver (Sigma-Aldrich). Samples were serially diluted in PBS and plated onto Todd Hewitt Agar (THA) plates. The final number of colony forming units (CFU) were counted the next day following an overnight incubation at 37°C.

2.3.3 Photobleaching of GFP-expressing S. aureus by neutrophils

This section has been reproduced in this current format from de Jong et al., Copyright © 2018, The American Society for Biochemistry and Molecular Biology, Inc.

The capacity of full-length SPIN and SPIN$^{46-105}$ to inhibit MPO activity within neutrophil phagosomes was examined. Human neutrophils were isolated from venous blood, as described previously [39]. Written consent was obtained from each volunteer in accordance with a protocol approved by the Institutional Review Board for Human Subjects at the University of Iowa. Isolated neutrophils were then fed opsonized cells of *S. aureus* strain USA300 expressing super folded GFP (MOI 1:1) as previously described [40], either in the absence or presence of 50 μM SPIN or SPIN$^{46-105}$. Samples identical to these except for the presence of 10 μM diphenyleneiodonium (DPI) were run in parallel and were included to inhibit NADPH oxidase-dependent bleaching of GFP [41]. After 10 min of phagocytosis, undigested bacteria were removed, and neutrophils laden with *S. aureus* were incubated at 37 °C for 0 or 120 minutes.

Samples were analyzed by flow cytometry for loss of GFP fluorescence, as previously reported [40]. The mean fluorescence intensity (MFI) for each sample was calculated as the geometric mean of the GFP-positive population multiplied by the percent of cells gated. The percent MFI was normalized to values obtained for DPI-treated neutrophils.

2.4 Crystallography and X-ray diffraction

As described further in Chapters 4 and 5, two different SPIN/MPO complexes were crystallized. Samples of the SPIN-*delphini* and SPIN-*aureus*$^{46\text{-}105}$ bound to recombinant human MPO (R&D Systems) were prepared by mixing stoichiometric amounts of each protein and concentrating to 5 mg/mL total protein complex in a buffer of 5 mM tris (pH 7.4), 50 mM NaCl.

Crystals of SPIN$^{46\text{-}105}$/rMPO complex were obtained as described for the SPIN/rMPO complex [1]. Single crystals were harvested and cryopreserved in precipitant solution supplemented with an additional 10% (v/v) peg-400. X-ray diffraction data were collected at 1.0 Å wavelength using beamline 22-BM of the Advanced Photon Source (Argonne National Laboratory).

A description of the cell constants, diffraction data quality, and properties of the final model for the SPIN$^{46\text{-}105}$/rMPO complex can be found in Table 4.2. The rMPO used for these structural studies binds SPIN similarly to native human MPO (Table 4.1), but has a lower occupancy of the heme prosthetic group when compared to MPO produced by human neutrophils. This resulted in weak electron density for the heme in the SPIN$^{46\text{-}105}$/rMPO co-crystal structure, and precluded inclusion of heme in the final crystallographic model.

For the SPIN-*delphini*/rMPO, initial crystallization trials were carried out by vapor diffusion of hanging drops at 20 ºC using Hampton Research Crystal Screen I and II and various customized buffers. Crystals suitable for X-ray diffraction studies were grown over the course of 7-10 days from drops that contained 1 μL of complex mixed with 0.5 μL distilled water and 0.5 μL of a precipitant solution consisting of 0.1 M sodium acetate (pH 4.6), 25% (v/v) PEG 3350.

The crystals were briefly soaked in a cryoprotectant solution of 0.1 M sodium acetate (pH 4.6), 25% (w/v) PEG 3350 and 10% (v/v) PEG 4000 prior to flash cooling in liquid N_2. X-ray diffraction data were collected at beamline 22-ID of the Advanced Photon Source of Argonne National Laboratory. A total of 360 images were collected with an oscillation angle of 1º, an exposure time of 1 s, radiation of λ=1.000 Å, and a sample to detector distance of 300 mm.

The reflections were indexed, integrated, and scaled using the HKL-2000 package [42]. The structure was solved by molecular replacement using and the refined polypeptide coordinates of SPIN-*aureus*/rhMPO (PDB entry 5UZU) as a search model [43] and PHASER [44] as implemented in the PHENIX software suite [45]. The final model was constructed by an iterative combination of automated and manual rebuilding, followed by crystallographic refinement using PHENIX.REFINE [45, 46].

For the SPIN-*delphini*/rMPO complex 96.08% of the modeled polypeptide residues lie in favored regions of the Ramachandran plot, with only 0.31% in regions classified as outliers. In addition to the two polypeptides, the final model contains 105 ordered solvent molecules, a Ca^{2+} ion coordinated entirely by groups derived from rhMPO, a single Cl^- ion, and a covalently bound heme prosthetic group within the MPO active site. A more detailed description of the cell constants, diffraction data quality, and properties of the final model can be found in Table 5.3.

On the other hand, in the $SPIN^{46-105}$/rMPO complex 94.26% of the modeled polypeptide residues lie in favored regions of the Ramachandran plot, with only 1.26% in regions classified as outliers.

All structural analyses, including calculation of buried surface areas and identification of potential hydrogen bonds and salt bridges, were performed using EBI-PISA (http://www.ebi.ac.uk/msd-srv/prot_int/cgi-bin/piserver). Representations of protein structures were generated by PyMol (http://www.pymol.org/).

2.5 Nuclear Magnetic Resonance

NMR is a technique with a vast literature used to investigate the structure and purity of chemical compounds and biomolecules based on the interaction of nuclear spins with a magnetic field. The sample is placed in a strong magnetic field and the NMR signal is produced by excitation of the nuclei sample with radio waves into nuclear magnetic resonance and detected with sensitive radio receivers.

The intramolecular magnetic field around atoms in a molecule influences the resonance frequency, giving access to details of the electronic structure of a molecule and to individual functional groups or residues. This can make NMR hard to interpret, as the positions of the resonances are affected by the structure of the molecule. Besides identification, NMR spectroscopy provides detailed information about the structure and dynamics of molecules. The most common types of NMR are proton and ^{13}C NMR spectroscopy, but it is applicable to any kind of sample that contains nuclei possessing spin. Most common nuclei studied by NMR are protons (spin ½), and a few other, spin -½ nuclei, such as ^{13}C and ^{19}F. The techniques are referred to the nuclei studied as ^{1}H NMR, ^{13}C NMR, etc.

With the increase in molecular weight, the number of peaks also increases, resulting in crowded and overlapped spectra, especially when monitoring proteins since they tumble slower in solution which results in broader peaks. To simplify the process of identification and assignment of residues we use different approaches as illustrated in Table 2.1.

Table 2.1 Resonance assignment strategies depend on the protein molecular weight.

Molecular weight	Isotopic labeling	Approach
≤ 8-10 kDa	None	^{1}H homonuclear (COSY/TOCSY + NOESY)
~ 8-25 kDa	Uniform ^{13}C, ^{15}N	Triple resonance
≥ 25 kDa	Uniform ^{13}C, ^{15}N, ^{2}H and/or selective labeling	^{2}H-modified triple resonance

Since SPIN-*aureus* is ~8.6 kDa (including an extra "Gly-Ser-Tyr" at the N-terminus), we used uniform ^{15}N and double ^{15}N/ ^{13}C labeling of the protein.

2.5.1 Sample preparation

All NMR measurements were performed at 25 ºC on either a Varian (Agilent Technologies) 500VNMR (499.84 MHz for 1H frequency) or a Bruker Avance (700.11 MHz for ^{1}H frequency) spectrometer, both of which were equipped with cryogenic probes. The ^{1}H chemical shifts were referenced to the external standard 2,2-dimethyl-2-silapentane-5-sulphonic acid (DSS) at 25 °C and the ^{13}C and ^{15}N chemical shifts were referenced indirectly from DSS.

The purified, isotopically-enriched SPIN proteins were dissolved at 0.75-1.0 mM final concentration in 50 mM sodium phosphate (pH 6.5) supplemented with 5% (v/v) D_2O as a lock solvent prior to spectral collection.

2.5.2 Experimental spectra collection

Backbone and sidechain resonances for SPIN were assigned through standard double and triple resonance spectra. Triple-resonance NMR spectra corresponding to HNCA, HN(CO)CA, HNCACB, CBCA(CO)NH, and HNCO were recorded on uniformly ^{15}N/^{13}C labelled SPIN samples to facilitate backbone assignment. Two-dimensional ^{13}C HSQC and three-dimensional

HCCONH, CCCONH, HCCH-TOCSY, 15N HSQC-TOCSY (tm=80 ms) and ^{15}N-edited NOESY (tm =100 ms) spectra were recorded for side chain assignment.

Longitudinal (R_1) and transverse (R_2) relaxation time constants for ^{15}N amide atoms were determined using the steady-state, inversion-recovery and Carr-Purcell-Meiboom-Gill methods respectively [47, 48]. For R_1 determination, ^{15}N-HSQC spectra with the following relaxation delays were collected: 0.03, 0.05, 0.07, 0.12, 0.15, 0.23, 0.35, 0.80, 1.00, 1.20, 15.0, and 1.80 s. For R_2 determination, ^{15}N-HSQC spectra with the following delays were collected: 0.03, 0.05, 0.07, 0.13, 0.15, 0.17, 0.19, 0.21, and 0.23 s.

The R_1 and R_2 time constants were calculated by measuring the intensity of the peak corresponding to each assigned ^{1}H-^{15}N pair from the ^{15}N-HSQC spectra and fitting the resulting decay as function of time delay (t) to a two-parameter exponential decay described by $I(t)=I_oe^{-tR}$, where I(t) is the intensity of the peak as a function of relaxation delay time t. I_o is the normalized peak intensity at t=0. All such calculations were performed using the Rate Analysis feature of NMRView 9.2 (One Moon Scientific, Westfield, NJ) [49].

NMR data were processed using NMRPipe [50], while spectra were analyzed and visualized using CARA (http://www.nmr.ch/) [51]. The chemical shift assignments have been deposited in the BioMagResBank (www.bmrb.wisc.edu/) under the accession number 27069 and described in more detail elsewhere [52].

The experimentally-derived chemical shift values for SPIN resonances were used to determine solution structural features of SPIN in the absence of MPO. The secondary structure

of SPIN was predicted using the TALOS-N platform [52, 53]. Likewise, the CS-Rosetta Server (Rosetta v3.8, CS-Rosetta Toolbox v3.3) was used to generate 40,000 independent models for three-dimensional structure of SPIN [54, 55] consistent with the chemical shift data. This approach was used because the NMR spectra collected on SPIN were not sufficient to permit experimental determination of its structure.

Chapter 3 - Backbone and side-chain ^{1}H, ^{15}N, and ^{13}C resonance assignments of a novel Staphylococcal inhibitor of Myeloperoxidase

Nicoleta T. Ploscariu[1], Alvaro I. Herrera[1], Srinivas Jayanthi[2], Thallapuranam K. Suresh Kumar[2], Brian V. Geisbrecht[1] and Om Prakash[1]

[1] *Department of Biochemistry and Molecular Biophysics, Kansas State University, Manhattan, KS 66506*

[2] *Department of Chemistry and Biochemistry, University of Arkansas, Fayetteville, AR 72701*

SPIN is a protein with no sequence homology to any known proteins. Solution NMR structural studies of SPIN are therefore expected to provide a deeper understanding of its interaction with MPO. In this subchapter, we report the backbone and side-chain ^{1}H, ^{15}N, and ^{13}C resonance assignments of SPIN. Furthermore, using the chemical shifts of these resonances, we predicted the secondary structure of SPIN in solution via the TALOS-N server. The assignment data has been deposited in the BMRB data bank under accession number 27069.

Staphylococcus aureus is a pathogenic bacterium known for its ability to cause a variety of infections such as endocarditis, skin abscesses and bacteremia [56, 57]. Previous studies have demonstrated that *S. aureus* produces an array of virulence proteins that disrupt normal function of the human innate immune system [58]. The combined activities of these proteins are believed to prolong bacterial survival within the host, allowing for infections to take hold.

Neutrophils are the most abundant type of white blood cells in humans and the most prominent cellular component of the innate immune system. They can be rapidly activated by various biochemical stimuli during the earliest phase of bacterial invasion and recruited into the sites of infection [59]. Neutrophils contain subcellular granules that are replete with vital anti-bacterial enzymes, including a series of chymotrypsin-like Neutrophil Serine Proteases (NSPs) as well as a heme-containing Myeloperoxidase (MPO) [6, 59]. Novel classes of *S. aureus* secreted proteins, such as the Extracellular Adherence Protein (EAP) family [26] and Staphylococcal Peroxidase Inhibitor (SPIN) proteins [1] have been identified as inhibitors of NSPs and MPO, respectively. Our understanding of the mechanisms used by neutrophils to eliminate pathogens continues to expand. While it has been long believed that neutrophils eliminate pathogens through phagocytosis alone, more recent work has shown that neutrophils can employ additional killing mechanisms such as degranulation and NETosis [6, 59, 60]. These mechanisms,

particularly the release of digestive and oxidative granular enzymes into the inflammatory environment, can expose otherwise healthy host cells and extracellular matrices to substantial damage. In the case of recurring infections, the immune response can lead to scar tissue and in some cases, even malignancy [61].

Since MPO is a vital component of neutrophil's anti-bacterial arsenal and is a major component of neutrophil granules, release of MPO into the extracellular space can result in production of damaging hypohalous acids. Characterization of novel classes of enzymatic inhibitors that target key enzymes within the neutrophil anti-bacterial repertoire may therefore open new directions for development of anti-inflammatory therapies.

Our previous studies have identified SPIN as the first described innate immune evasion protein that acts as an exclusively specific inhibitor of MPO. SPIN binds MPO with nanomolar affinity (K_D ~10 nM) and a crystal structure of the complex has been obtained [1]. While the structure of SPIN in bound form is predominantly characterized by a three-helix bundle, an ~10 residue region at its N-terminus adopts a peculiar beta hairpin conformation that inserts into the MPO active site channel. Preliminary analyses have revealed that loss of this N-terminal region dramatically reduces SPIN's ability to inhibit MPO without any notable effect on its K_D value. As a prelude to detailed structure/function studies, we investigated herein the secondary structural features of SPIN in the free form in solution. After assigning the backbone and side-chain ^{1}H, ^{15}N, and ^{13}C resonances of SPIN, we were able to predict the secondary structure using TALOS-N server using the observed chemical shifts.

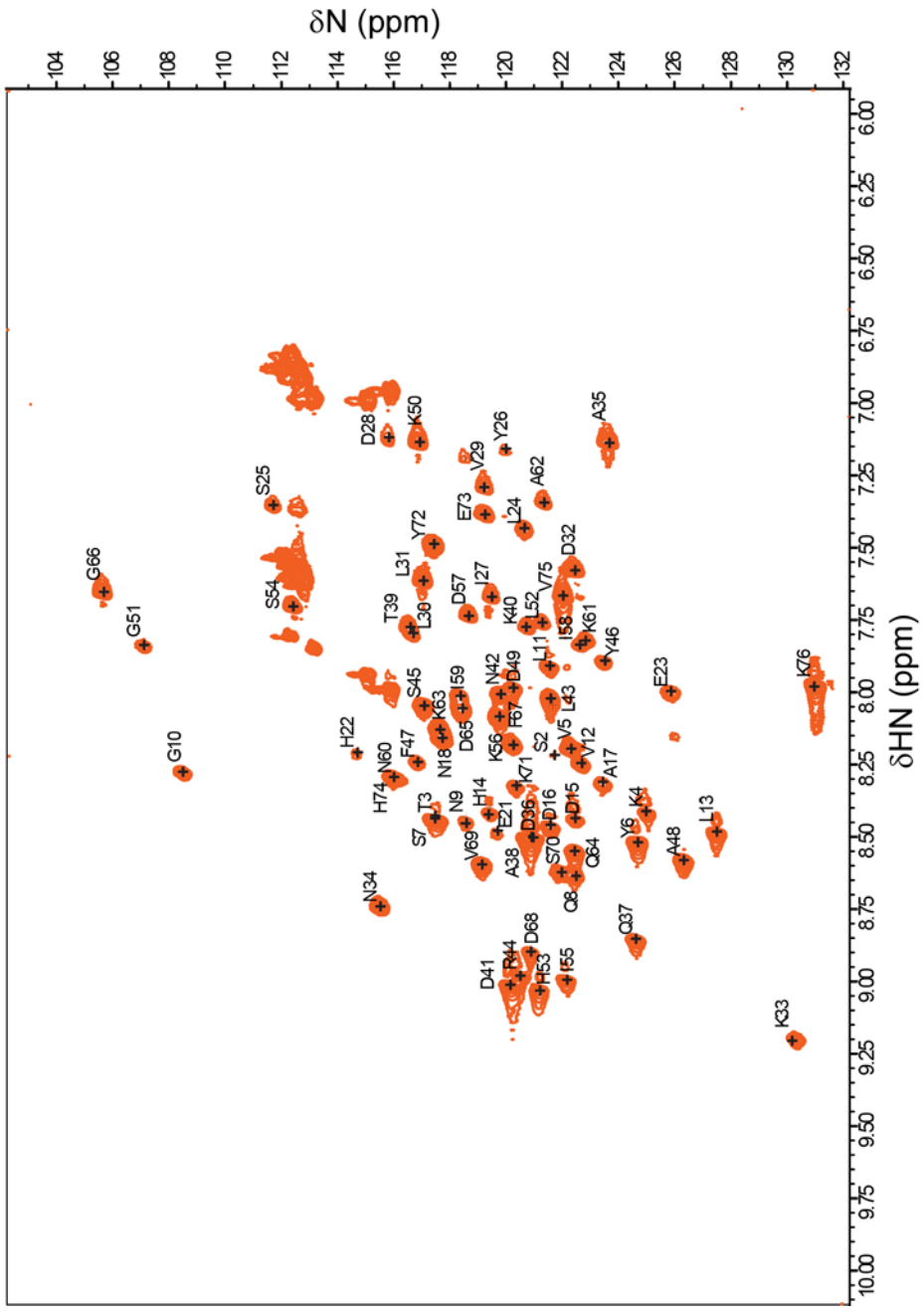

Figure 3.1 The 2D ^{1}H - ^{15}N HSQC spectrum of 1 mM of $^{13}C/^{15}N$-labeled SPIN recorded at 25ºC on Bruker Avance 700 MHz spectrometer. The residues were labeled from 1 to 75, corresponding to the sequence numbering from 30 to 105.

Extent of the assignments and data deposition

As illustrated in Fig. 3.1, the 2D $^{1}H–^{15}N$ HSQC measurement of SPIN resulted in a well-dispersed spectrum. The unlabeled peaks in this figure belong to the side chains of Asn and Gln residues. Amino acid numbering is based on the SPIN sequence, including the N-terminal "Gly-Ser-Thr". For the purpose of this study, the residues were assigned numbers from 1 to 75 and the equivalent residue number in the mature form of SPIN is found in the schematic in figure 3.2. The sequence specific backbone resonance assignments for nearly all ^{1}H, ^{15}N and ^{13}C spins were completed (97% $^{1}H/^{15}N$ assignments) using the NMR experiments described in the Chapter 2, NMR section. The backbone amide protons that could not be assigned include F^{19} and L^{20}. Based on secondary structure prediction, these unassigned residues are located on the C-terminus of a dynamic region (1-20AA) connecting to an alpha-helix (21-32AA) and probably could not be identified due overlap or line-broadening of the relevant Cα and Cβ resonances.

Spin resonances for HN, N, Cα, Cβ, Hα, Hβ and C were assigned for >95% of the residues. The analysis of HN(CO)CA, HNCACB, CBCA(CO)NH, and HNCO resulted in the assignment of 95% of $^{13}C\alpha$ resonances, 92% of $^{13}C\beta$ resonances, and 76% of all ^{13}C resonances. The chemical shift assignments have been deposited in BioMagResBank (www.bmrb.wisc.edu) under the accession number 27069.

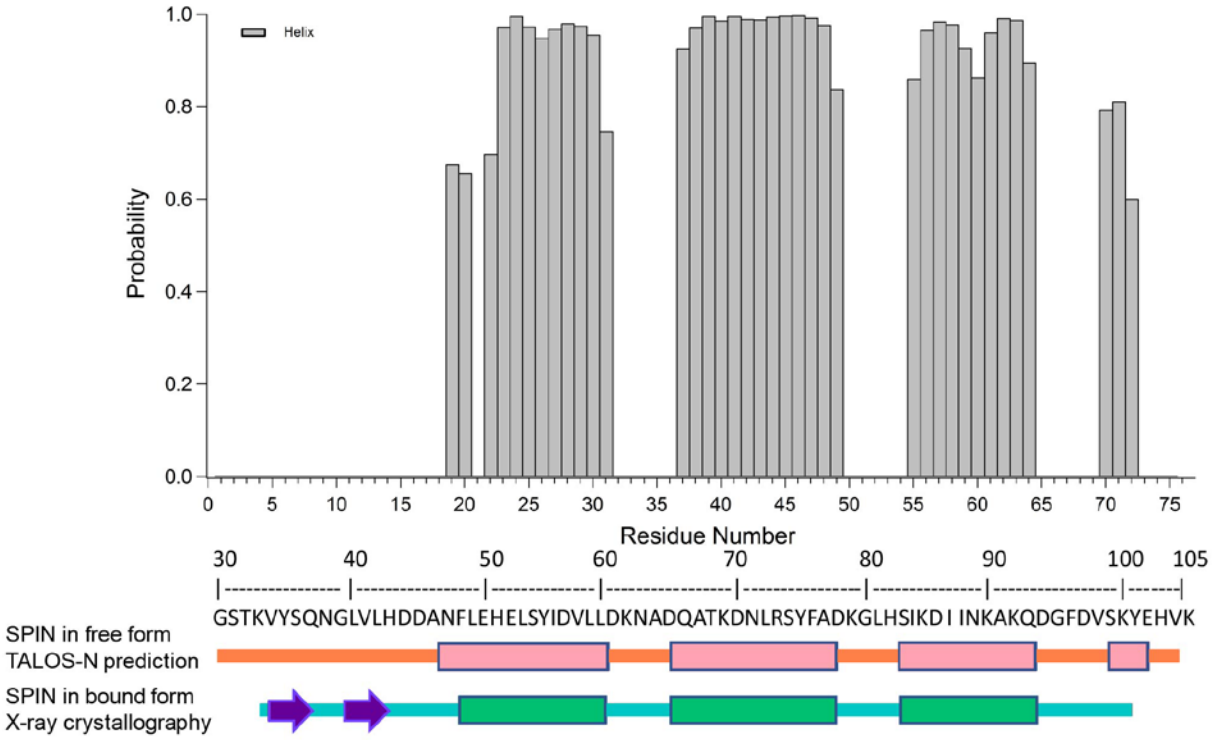

Figure 3.2 TALOS-N prediction based on chemical shift values of $^{13}C\alpha$, $^{13}C\beta$, and ^{13}C, NH and ^{1}H. Below is represented a schematic of secondary structure (rectangle = alpha helix, arrow =beta strand) of the TALOS-N prediction of SPIN in free form and of the crystal structure of SPIN in bound form.

The secondary structure of SPIN was predicted by TALOS-N program [53] using the resonance assignments of $^{13}C\alpha$, $^{13}C\beta$, and ^{13}C, NH and ^{1}H (Fig. 3.2). We compared this predicted secondary structure of SPIN in the free form in solution with the one determined by X-ray crystallography for SPIN bound to recombinant human MPO [1]. Although the SPIN-MPO co-crystal structure shows that N-terminal region of SPIN adopts a β-hairpin, TALOS-N prediction of the free SPIN in solution suggests that this region is not similarly structured in the unbound protein. Additional studies are underway to further investigate the structure/function consequences of this discrepancy.

Chapter 4 - A Structurally Dynamic N-terminal Region Drives Function of the Staphylococcal Peroxidase Inhibitor (SPIN)

Nienke W.M. de Jong[1,*], Nicoleta T. Ploscariu[2,*], Kasra X. Ramyar[2], Brandon L. Garcia[2], Alvaro I. Herrera[2], Om Prakash[2], Benjamin B. Katz[2], Kevin G. Leidal[3], William M. Nauseef[3], Kok P.M. van Kessel[1], Jos A.G. van Strijp[1], and Brian V. Geisbrecht[2]

[1]Medical Microbiology, University Medical Center Utrecht, 3584 CX Utrecht, The Netherlands;

[2]Dept. of Biochemistry & Molecular Biophysics, Kansas State University, Manhattan, KS 66506, USA;

[3]Inflammation Program, Department of Internal Medicine, Roy J. and Lucille A. Carver College of Medicine University of Iowa, †Veterans Administration Medical Center, Iowa City, IA 52240

Introduction

In this chapter we present the outcome of a series of experiments designed to assess the structure/function relationships of SPIN. We initially carried out a solution NMR study to characterize the SPIN N-terminus in the absence of MPO. We then prepared and characterized a panel of deletion and site-directed mutants of SPIN to define the contributions of its two discrete regions in MPO binding and inhibition. Together, our results suggest that the SPIN N-terminus is dynamically structured in the absence of MPO, but absolutely required to inhibit MPO activity even though it contributes only minimally to binding. Intriguingly, we found that the SPIN N-terminus is susceptible to site-specific proteolysis by NSPs, but protected in the presence of *S. aureus* EAP proteins. This suggests that functional synergy may exist between these two distinct classes of intracellularly-acting evasion proteins. Collectively, our data provide insights into SPIN structure/function relationships and deepen our appreciation of the biomolecular events that underlie *S. aureus* innate immune evasion.

The N-terminal Region of SPIN is Dynamically Structured in the Absence of MPO

Although we previously solved a 2.4 Å resolution crystal structure of SPIN bound to rMPO, our attempts to crystallize SPIN on its own were unsuccessful. We therefore explored solution NMR spectroscopy as an alternative approach to obtain insight into the structure of SPIN in its unbound state. Since the ^{1}H-^{15}N HSQC spectrum of isotopically-enriched SPIN exhibited excellent dispersion (Figure 4.1), we collected the standard suite of two- and three-dimensional NMR spectra to permit assignment of the SPIN backbone resonances [52]. Initially, 97% of the resonances identified in the ^{1}H-^{15}N HSQC spectrum collected at 700 MHz were assigned, leaving only those arising from Phe^{48} and Leu^{49} unaccounted for. These chemical shift

assignments have been deposited in the BioMagResBank (accession number 27069), and were described in Chapter 3 [52].

We used the TALOS-N platform to calculate the secondary structure of SPIN on the basis of backbone chemical shift values [53], and additionally determined both the longitudinal (R_1) and transverse (R_2) relaxation rates for the backbone resonances assigned in the ^{1}H-^{15}N HSQC spectrum (Fig. 4.2A-C). Since the relaxation data were recorded on a 500 MHz spectrometer, we collected an additional ^{1}H-^{15}N HSQC spectrum at this lower field strength; due to the decreased resolution at 500 MHz, the resonances of Gln^{37} and Glu^{50} were no longer detected. From these data, we inferred that the four unassigned residues from the SPIN backbone (i.e. Gln^{37}, Phe^{48}, Leu^{49}, and Glu^{50}) are all located within an apparently flexible region that comprises the N-terminus up to the start of the first α-helix (i.e. His^{51}-Asp^{61}). For internally rigid proteins, the values of R_1 and R_2 are expected to have homogeneous values. However, we found that the N-terminal residues of SPIN displayed higher and lower values for R_1 and R_2, respectively, when compared to the entire protein on average. For these parameters, deviation from the average is often associated with sites that present backbone flexibility and undergo fast internal dynamics [62]. In the case of SPIN, the overall average value for R_1 was 2.49±0.58 with a higher value of 2.90±0.78 for the N-terminal region, while R_2 rates overall averaged 8.97±1.29 with a lower value of 7.64±1.33 in the N-terminal region. Similarly, the overall average value of R_2/R_1 was 3.72±0.73, while residues found in the N-terminal region averaged 2.76±0.59.

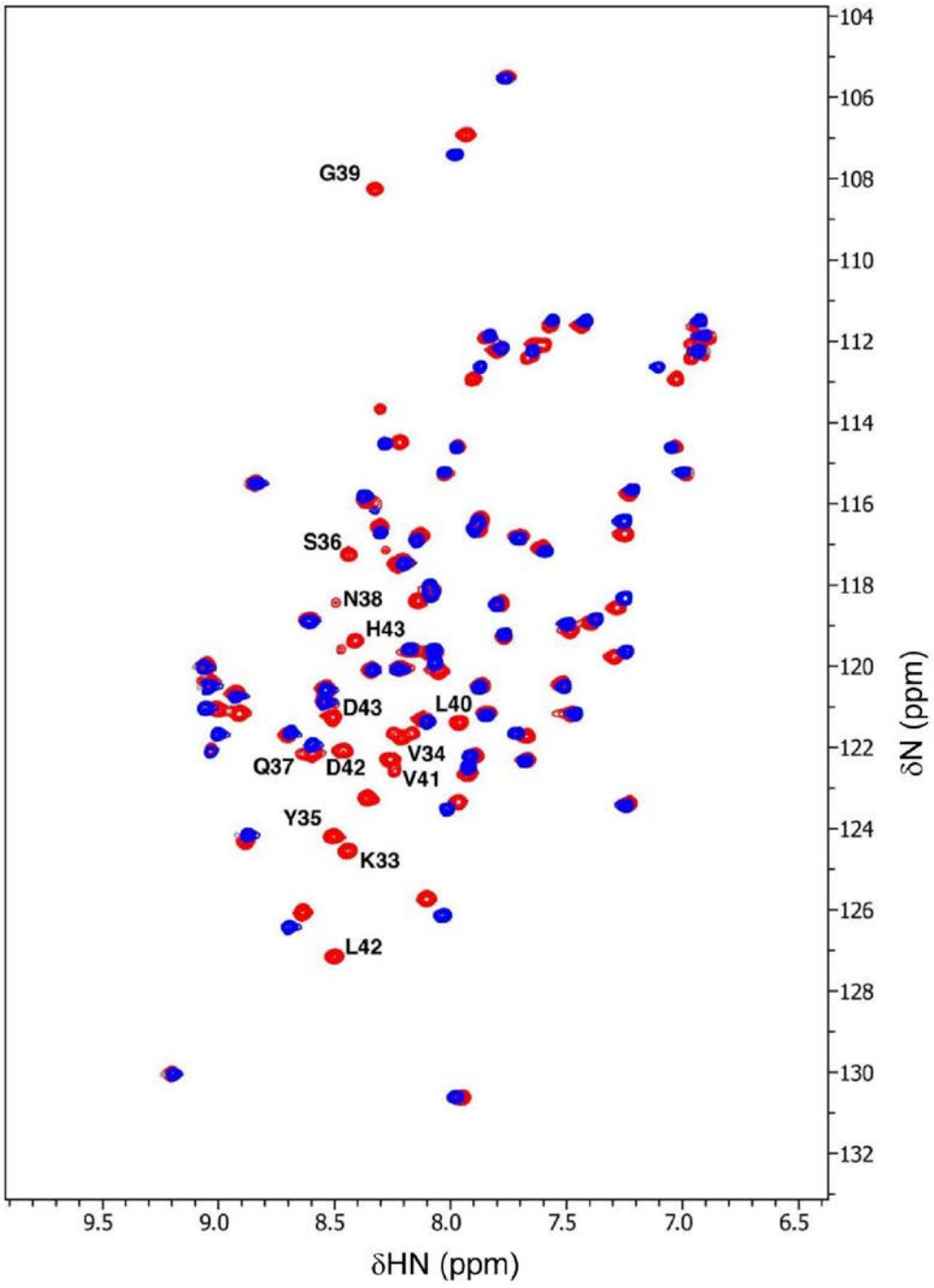

Figure 4.1 Comparison of $^{1}H^{15}N$-HSQC Spectra of 15N-labeled full-length SPIN (red) and $SPIN^{46-105}$ (blue) recorded at 25 ºC on a Varian 500VNMR Spectrometer. The labels represent resonances corresponding to residues found within the N-terminal region of the SPIN protein.

To gain further insight into the solution structure of SPIN, we also collected three-dimensional HCCONH, CCCONH, HCCH-TOCSY, ^{15}N HSQC-TOCSY and ^{15}N-edited NOESY spectra to facilitate sidechain assignments. These efforts resulted in assignment of 95% of the $^{13}C_{\alpha}$ resonances and 92% of the $^{13}C_{\beta}$ resonances for SPIN [52]. We compared the chemical shift index (CSI) values for these SPIN resonances to the BMRB statistical database values for CSI (Fig. 2D, E). For these parameters, residues that approach a neutral CSI value are associated with a random-coil like structure [63]; residues within α-helical structure have high positive values for C_{α} and high negative values for C_{β}, while residues within β-strands are characterized by negative values for C_{α} and positive values for C_{β} [63]. Significantly, the CSI variance for residues in the SPIN N-terminal region was markedly lower than that of the protein overall, and was consistent with the absence of regular secondary structure.

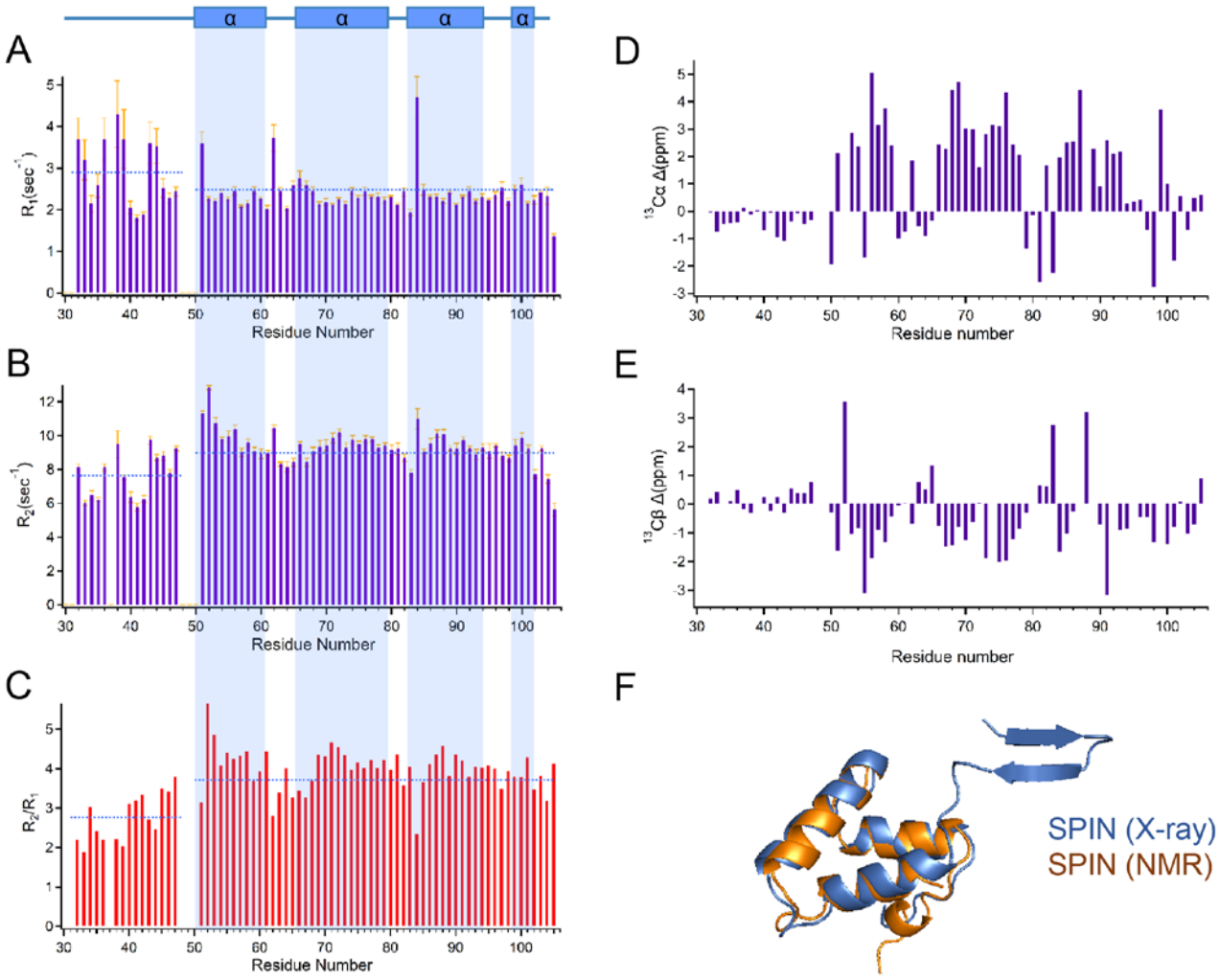

Figure 4.2 The N-terminal Region of SPIN is Dynamically Structured in the Absence of Ligand. NMR spectroscopy was used to characterize the solution structure of SPIN in the absence of MPO. A series of solution dynamics studies were performed following assignment of the resonances identified in a 1H-15N HSQC spectrum of isotopically-enriched SPIN. A summary of 15N (A) longitudinal (R1) relaxation time constants, (B) transverse (R2) relaxation time constants, and (C) R2/R1 values are presented as a measure of site-specific rotational diffusion motion. The highlighted regions (light blue) illustrate the TALOS-N prediction of SPIN secondary structure in the free form based upon NMR chemical shift data, as represented above the top of panel in rectangular boxes (alpha helical regions). The mean value for each parameter (R1, R2, or R2/R1) for residues within either the N-terminal region or the protein overall is represented a dashed blue line. Chemical Shift Index variance plots for (D) Cα and (E) Cβ resonances, respectively. The values were calculated as the difference between the experimentally determined chemical shift and BMRB statistical chemical shift values for residues found in unstructured regions. (F) Three-dimensional superposition of MPO-bound SPIN and a chemical shift-derived model for SPIN in the solution state. The model in blue represents the bound form of SPIN as determined by the SPIN/rMPO crystal structure, while the model in orange represents the structure of SPIN calculated by the Chemical Shift Rosetta server derived from solution NMR measurements.

Finally, we used the CS-Rosetta server to calculate an ensemble of 40,000 three-dimensional structural models compatible with the SPIN chemical shift data. Comparison of the entire ensemble versus the lowest-energy structure gave an RMSD of 1.134±0.321 Å. When we carried out similar calculations using an option where flexible regions were truncated automatically (i.e. residues 33-53), the RMSD of the ensemble relative to the lowest-energy structure was 0.796±0.163 Å. Superposition of this lowest-energy model onto the structure of MPO-bound SPIN [1] yielded an RMSD of 1.470 Å for all backbone atoms, and demonstrated otherwise good agreement between structural data obtained for the α-helical bundle region SPIN in solution versus the crystalline form (Fig. 4.2F). In summary, while SPIN in the bound state displays a β-hairpin structure at its N-terminus, our studies presented here strongly suggest that this region is dynamic and has a random coil character prior to MPO binding.

The N-terminal Region of SPIN is Dispensable for MPO Binding

The crystal structure of SPIN bound to rMPO identified two distinct interaction sites that buried approximately 1600 $Å^2$ of total surface area [1], as judged by the EBI-PISA server [64]. Although the SPIN/rMPO interface is contiguous on the SPIN surface, it is useful for purposes of analysis to consider its comprised of two distinct binding sites [1]. The first site accounts for ~45% of the buried SPIN surface area and is derived from residues within the α-helical bundle; the second binding site accounts for the remaining ~55% of buried SPIN surface area and arises from residues within the N-terminal β-hairpin [1]. The number of potential hydrogen bonds and salt bridges at the SPIN/rMPO interface is distributed roughly equally across the two binding sites, although the α-helical bundle appears to contribute more hydrogen bonds and the β-hairpin seems to predominate in salt bridges. Given the inconclusive nature of this interface analysis, we

determined that structural information alone could not be used to establish which binding site was more important to forming and/or maintaining the SPIN/rMPO interaction. However, since the N-terminal β-hairpin of SPIN does not appear to form until after MPO binding has occurred (Fig. 4.2), we hypothesized that the α-helical bundle site might be of primary importance in initially binding to MPO.

To test this hypothesis, we prepared and characterized both a deletion and site-directed mutant that altered the SPIN N-terminus (Figs. 4.1, 4.3). The deletion mutant removed the entire N-terminal region and consisted of residues Ala^{46}-Lys^{105} inclusive (i.e. $SPIN^{46}$-^{105}). The site-directed mutant was prepared to assess the contributions of His^{43}, Asp^{44}, and Asp^{45}, and exchanged each of these residues for Ala in the full-length SPIN background (i.e. $SPIN^{43-45\rightarrow AAA}$). These residues are essentially invariant across representative SPIN sequences from non-*aureus Staphylococcus* spp. and also form salt bridges with MPO sidechains in the SPIN/rMPO co-crystal structure [1].

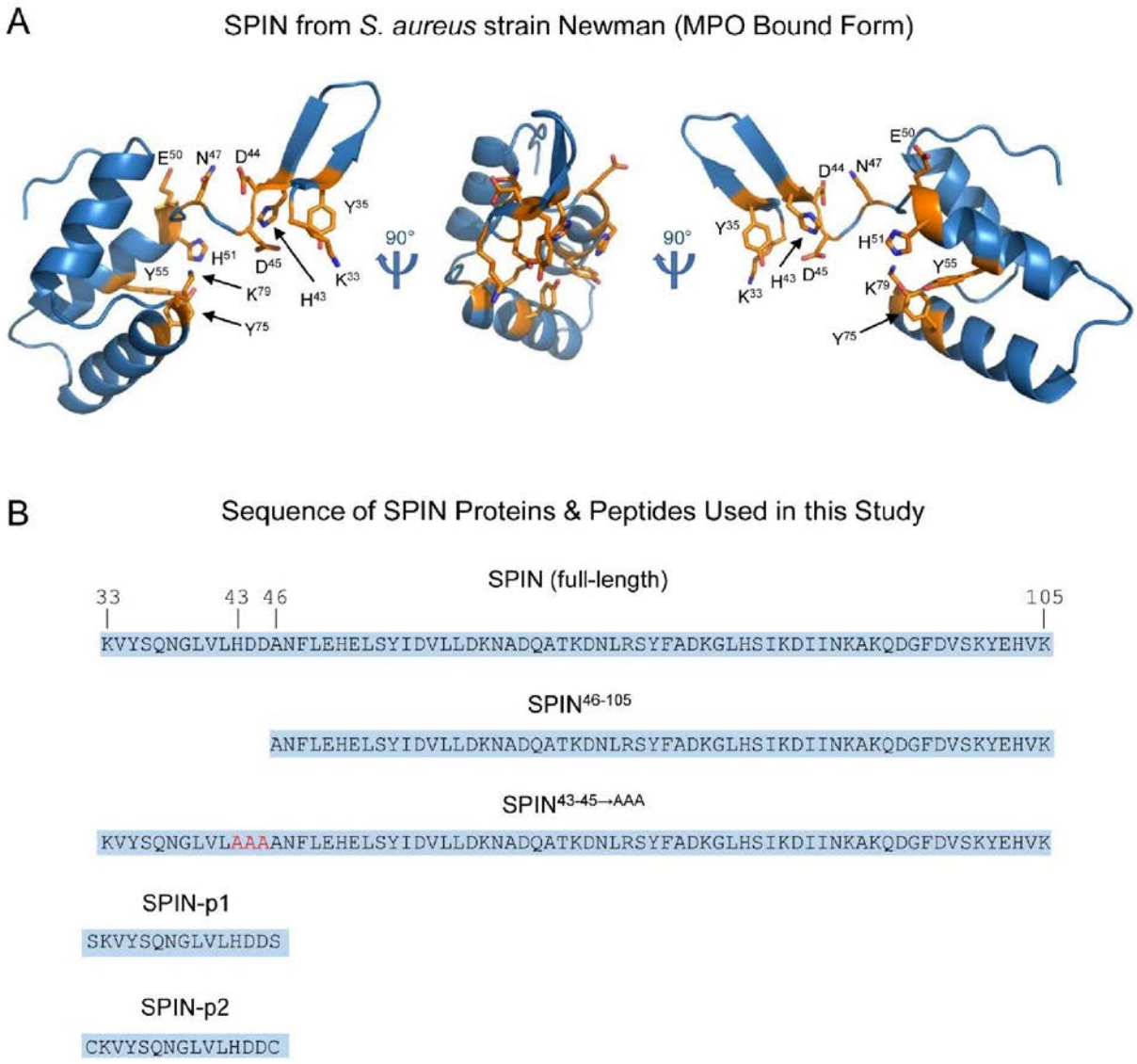

Figure 4.3 Structure of *S. aureus* SPIN and Sequences of SPIN Proteins Used in this Study. (A) Three different views of the MPO-bound *S. aureus* SPIN structure (PDB entry 5UZU). The SPIN protein is drawn as a blue ribbon. Residues whose sidechains participate in either hydrogen bonds or salt bridges with MPO are drawn in stick convention, with carbon atoms colored orange, nitrogen in dark blue, and oxygen in red. The labels of these residues reflect the values shown in panel B below. (B) The sequences of recombinant proteins and synthetic peptides used in this study are presented above. The full-length SPIN sequence from *S. aureus* strain Newman is shown at the top. Numbering reflects those residues found in the matured polypeptide following removal of the secretion signal sequence. Letters shown in red typeface indicate the positions altered by site-direction mutations.

We examined the ability of these SPIN mutants to bind both native MPO as well as a recombinant form of human MPO (rMPO) using a surface plasmon resonance approach (Fig. 4.4A-C).

Table 4.1 Surface Plasmon Resonance Assessment of SPIN Proteins Binding to Various Forms of MPO

Analyte	Surface	K_D (nM)	k_{on} ($M^{-1}s^{-1}$)	error k_{on} ($M^{-1}s^{-1}$)	k_{off} (s^{-1})	error k_{off} (s^{-1})	χ^2
SPIN	Native MPO	9.3	$5.37*10^5$	$3.5*10^3$	$4.99*10^{-3}$	$3.0*10^{-5}$	0.148
SPIN	Human rMPO	11.8	$4.46*10^5$	$1.5*10^3$	$5.24e*10^{-3}$	$1.5*10^{-5}$	0.128
$SPIN^{46-105}$	Native MPO	29.8	$6.19*10^5$	$2.3*10^3$	$1.85*10^{-2}$	$3.0*10^{-5}$	0.102
$SPIN^{46-105}$	Human rMPO	35.1	$4.30*10^5$	$1.2*10^3$	$1.51*10^{-2}$	$2.0*10^{-5}$	0.067
$SPIN^{43-45\rightarrow AAA}$	Native MPO	31.4	$5.27*10^5$	$3.3*10^3$	$1.65*10^{-2}$	$1.0*10^{-4}$	0.170
$SPIN^{43-45\rightarrow AAA}$	Human rMPO	32.6	$4.88*10^5$	$1.2*10^3$	$1.59*10^{-2}$	$1.8*10^{-5}$	0.043

We found that $SPIN^{46-105}$ was approximately 3.2-fold weakened in its K_D value for native human MPO relative to full-length SPIN (Table 4.1). Similarly, $SPIN^{43-45\rightarrow AAA}$ has a 3.4-fold diminished K_D for native human MPO (Table 4.1). For both mutants, the decreased affinity for MPO was associated with an enhanced dissociation rate of its complex with MPO relative to wild-type SPIN. Nevertheless, these mutants still bound MPO with low nanomolar K_D values near 30 nM, and retain the potent MPO-binding capacity intrinsic to wild-type SPIN [1]. This latter feature was reflected in a 2.3 Å resolution crystal structure of $SPIN^{46-105}$ bound to rMPO, which we solved and refined to R_{work}/R_{free} values of 17.9 and 22.9%, respectively (Fig. 4.4D and Table 4.2). In this regard, the structure of $SPIN^{46-105}$/rMPO is largely indistinguishable from SPIN/rMPO, as the Cα positions from the two models superimpose with an RMSD of 0.16 Å (Fig. 4.4E).

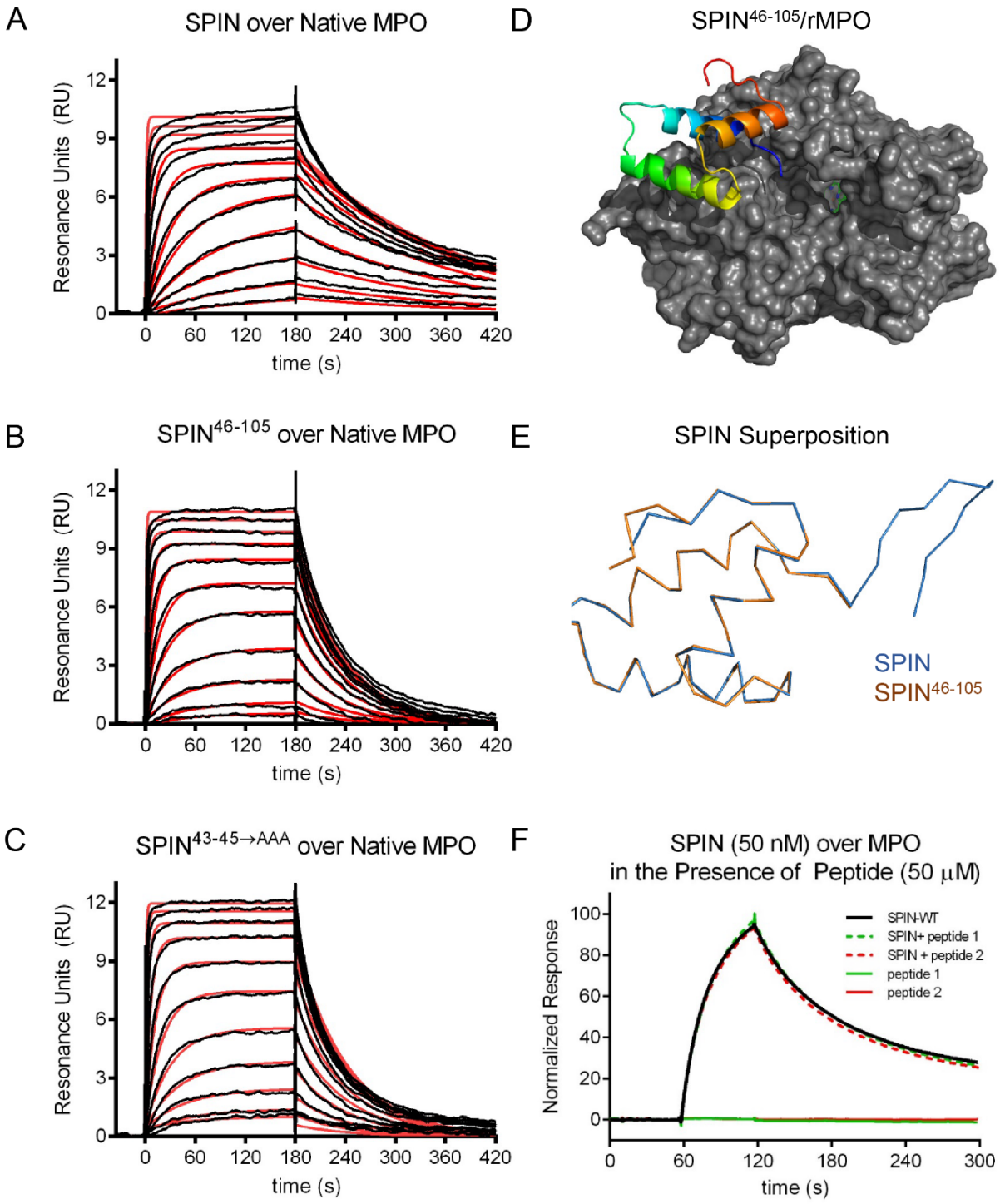

Figure 4.4 The N-terminal Region of SPIN is Dispensable for Binding to MPO. The ability of SPIN proteins and SPIN-derived peptides to bind MPO was examined using a combination of biochemical and structural methods. A two-fold dilution series of SPIN proteins ranging from 1.35 to 2000 nM was injected over a biosensor surface of prepared from randomly immobilized MPO. Representative sensorgram series are shown for native MPO binding to (A) full-length SPIN, (B) $SPIN^{46-105}$, and (C) $SPIN^{43-45\rightarrow AAA}$. Additional curve fitting and analysis parameters are presented in Table 4.1. (D)

Representation of a 2.3 Å resolution co-crystal structure of $SPIN^{46-105}$ bound to a recombinant form of human MPO. $SPIN^{46-105}$ is depicted as a ribbon diagram and is colored with its N-terminus in blue and its C-terminus in red, while MPO is rendered as a grey surface. The location of the MPO active site heme is indicated by a green ball-and-stick for the purposes of reference. (E) Superposition of the MPO-bound forms of $SPIN^{46-105}$ and full-length SPIN, as judged by X-ray crystallography. Proteins are depicted as wire diagrams, where the N-terminal β-hairpin of full-length SPIN is shown at the top right of the panel. (F) The MPO binding properties of two different synthetic peptides corresponding to SPIN N-terminal region were assessed by SPR. Peptide binding was investigated using both a direct binding approach (single injection at 50 μM) and through a competition format where peptides were co-injected along with SPIN (50 nM). Neither approach showed any evidence for binding between these peptides and MPO. A representative sensorgram series is shown.

Our studies with these SPIN mutants indicated that the N-terminal region of SPIN is dispensable for MPO binding. However, to examine this issue through an alternative approach, we synthesized two short peptides designed to mimic the SPIN N-terminus (Fig. 4.2). The first such peptide corresponded to the 13 N-terminal-most residues of SPIN (i.e. SPIN-p1), flanked by two Ser residues. The second contained the same residues as the first, plus a pair of Cys at the respective termini (i.e. SPIN-p2) that were oxidized to constrain the peptide into the β-hairpin conformation adopted by this region in the SPIN/rMPO crystal structure [1]. Due to the small size of these peptides, we examined their MPO binding properties through both conventional SPR methods as well as a competition-based assay wherein wild-type SPIN would be impeded from binding to the immobilized MPO surface. We found that neither SPIN-p1 nor SPIN-p2 gave evidence for direct or competitive binding to MPO at concentrations up to 50 μM (Fig. 4.4F). Thus, the experiments with these synthetic peptides were consistent with our mutagenesis and crystallographic studies in defining the α-helical region as the primary MPO binding site of SPIN.

Table 4.2 X-ray Diffraction Data Collection and Refinement Statistics

	$SPIN^{46-105}$/rMPO
Data Collection	
Space group	*C* 1 2 1
Cell dimensions	
a, *b*, *c* (Å)	128.85 92.88 80.46
α, β, γ (°)	90.00 119.91 90.00
Resolution (Å)	38.96-2.29 (2.38-2.29)
R_{pim}	0.063 (0.414)
$I / \sigma I$	12.0 (2.2)
Completeness (%)	99.0 (98.3)
Redundancy	7.7 (7.1)
Refinement	
Resolution (Å)	38.96-2.29
No. reflections	36,470
R_{work} / R_{free}	17.9/22.9
No. atoms	
Protein	5082
Ligand/ion	68
Water	282
B-factors	
Protein	41.95
Ligand/ion	62.87
Water	38.18
R.m.s. deviations	
Bond lengths (Å)	0.011
Bond angles (°)	1.136

*Values in parentheses are for highest-resolution shell.

The N-terminal Region of SPIN is Necessary, but Not Sufficient for Inhibition of MPO

Whereas the SPIN N-terminus could be removed from the protein with only an ~3 fold loss of affinity for MPO, the SPIN/rMPO crystal structure suggests that this region of SPIN likely makes important contributions to inhibition of MPO [1]. Moreover, while the α-helical region of SPIN is responsible for MPO binding (Fig. 4.4 and Table 4.1), it remained unknown if this portion of SPIN retained any MPO inhibitory capacity on its own. To investigate these questions, we characterized our SPIN mutants using an MPO activity assay wherein H_2O_2 reduction was linked to oxidation of o-dianisidine [1]. Since previous analysis of our SPIN mutants showed that they had essentially similar affinities for MPO (Table 4.1), we used a single

concentration for each potential inhibitor (i.e. 74 nM) sufficiently higher than the K_D to ensure high occupancy of the respective complexes. Whereas full-length SPIN significantly inhibited MPO activity under these conditions, we found that $SPIN^{46-105}$ failed to inhibit MPO when compared to the negative control protein, BSA (Fig. 4.5A). Intriguingly, $SPIN^{43-45\rightarrow AAA}$ also failed to block MPO activity, even though this mutant binds MPO with a K_D~30 nM and has a full length N-terminal region (Fig. 4.3).

As an independent test of SPIN function, we examined the effects of our mutants in an *in vitro* assay designed to replicate HOCl-dependent killing of bacteria within the phagosomal compartment [1, 65]. In this model, the enzyme glucose oxidase (GO) is employed as a surrogate H_2O_2-generating system for MPO in lieu of the multipartite NADPH-oxidase that assembles within the phagosomal membrane. Whereas full-length SPIN added *in trans* increased bacterial survival, neither $SPIN^{46-105}$ nor $SPIN^{43-45\rightarrow AAA}$ had any significant influence on the killing of *S. aureus* via bactericidal levels of HOCl generated by MPO (Fig. 4.5B). By contrast, the MPO inhibitor 4-ABAH restored the survival of the bacteria to normal levels. A similar trend was also seen in a neutrophil bleaching assay, which measures the loss of fluorescence by GFP-expressing *S. aureus* cells following phagocytosis [40]. Here, full-length SPIN added *in trans* significantly preserved the bacterially-derived GFP signal, while neither $SPIN^{46-105}$ (Fig. 4.5C) nor $SPIN^{43-45\rightarrow AAA}$ (Fig. 4.5D) added at an identical concentration were significantly more effective than buffer control. The slight reduction in bleaching observed for both $SPIN^{46-105}$ and $SPIN^{43-45\rightarrow AAA}$ likely resulted from these proteins acting competitively as a target for HOCl, rather than as inhibitors of MPO activity *per se* (Fig. 4.5A, C-D). Together, these results established that the N-terminal region of SPIN is necessary, but not sufficient for blocking MPO activity even though it makes only relatively minor contributions to MPO binding.

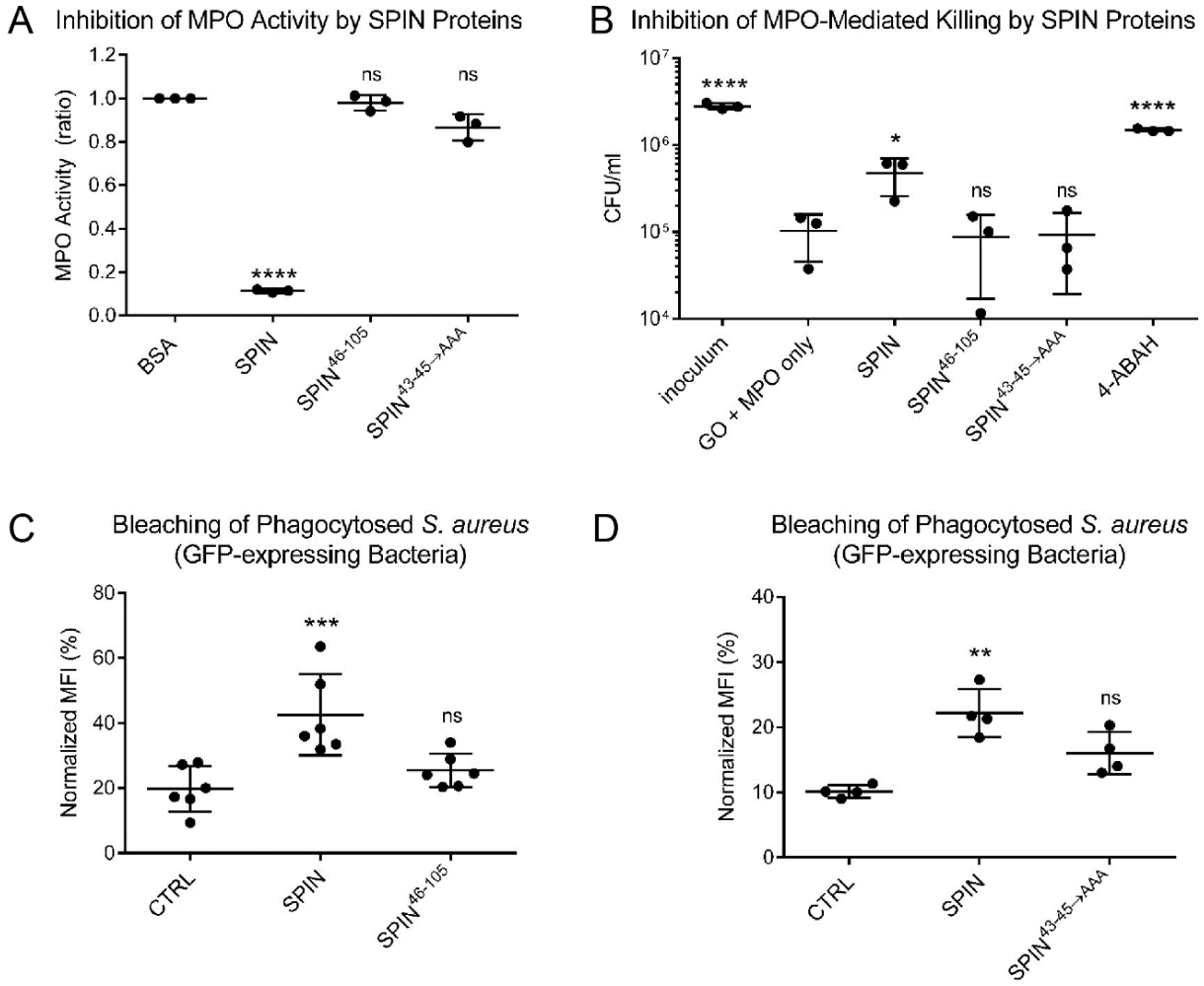

Figure 4.5 The N-terminal Region of SPIN is Necessary, but Not Sufficient for Inhibition of MPO. The functional consequences of deletion or mutation within the SPIN N-terminal region were assessed using two independent assay formats. (A) The effect of SPIN proteins on MPO activity was investigated using a spectrophotometric assay. Various SPIN proteins (74 nM final concentration) were incubated with MPO for 1 h prior to addition of a substrate mixture. Peroxidase activity was then measured at $OD_{450\ nm}$ relative to a negative control. Although full-length SPIN inhibits MPO activity, loss of either the entire N-terminus ($SPIN^{46\text{-}105}$) or positions 43-45 ($SPIN^{43\text{-}45\rightarrow AAA}$) rendered SPIN inactive. Significance relative to the negative control was determined by one-way ANOVA with Dunnett post-test correction for multiple comparison. Bars express SD with N=3. (B) The influence of SPIN proteins on a coupled glucose oxidase-MPO system that kills *S. aureus* strain Newman was also investigated. Whereas addition of full-length SPIN protects *S. aureus* from MPO-dependent killing, neither $SPIN^{46\text{-}105}$ nor $SPIN^{43\text{-}45\rightarrow AAA}$ retained this property, as judged by recovery of CFU counts compared to 'GO+MPO only'. As a control, the MPO inhibitor 4-aminobenzoic acid hydrazide (4-ABAH) also led to *S. aureus* survival. Significance relative to 'GO+MPO only' (a negative control for inhibition) was determined by one-way ANOVA with Dunnett post-test correction for multiple comparison. Bars express SD with N=3. (C) *S. aureus* cells constitutively expressing a cytosolic form of GFP were opsonized by human serum and incubated with 50 µM SPIN, 50 µM $SPIN^{46\text{-}105}$, or buffer alone (ctrl). The mixture of opsonized bacteria was added to freshly isolated human neutrophils to allow for phagocytosis to occur. The geometric mean of MFI for each sample was determined by flow cytometry at 2 hrs following inception of phagocytosis and

normalized to the signal for DPI-treated neutrophils at time zero. Whereas full-length SPIN significantly protected the GFP-expressing *S. aureus* cells from MPO-mediated bleaching, $SPIN^{46-105}$ gave only a slight, though not significant protection against bleaching relative to control. Levels of significance relative to buffer control were determined by one-way ANOVA with Dunnett post-test correction for multiple comparison. Bars express SD with N=6. (D) An analogous experiment to that shown in panel C, except that the properties of 50 µM SPIN, 50 µM $SPIN^{43-45\rightarrow AAA}$, or buffer alone (ctrl) were compared. $SPIN^{43-45\rightarrow AAA}$ gave only a slight, though not significant protection against bleaching relative to control. Levels of significance relative to buffer control were determined by one-way ANOVA with Dunnett post-test correction for multiple comparison. Bars express SD with N=4. Since $SPIN^{46-105}$ and $SPIN^{43-45\rightarrow AAA}$ do not inhibit MPO in activity (panel A) or killing assays (panel B), the signal observed in panels C and D likely reflects competition between the inactive SPIN protein and GFP for reaction with HOCl generated in the phagosome, thereby blocking bleaching of GFP indirectly. Experiments in panels C and D are presented separately due to variability in the assay, as they were conducted with neutrophils isolated at different times from different donors. * $p \leq 0.05$, ** $p \leq 0.01$, *** $p \leq 0.001$, **** $p \leq 0.0001$, ns (non-significant).

The N-terminal Region of SPIN is a Target for Degradation by NSPs

The phagosomal compartment matures in a step-wise fashion following uptake of opsonized bacteria. Early on in this process, azurophilic granules fuse with the phagosome whereby their contents are released into its lumen. This results in the accumulation of high levels of antimicrobial enzymes in the phagosome, with concentrations of MPO estimated to approach 1 mM [8]. Concentrations in this range have also been proposed for NSPs [66-69], which render the maturing phagosomal compartment not only highly oxidizing, but exceptionally digestive in character. In light of this, the dynamically-structured nature of the SPIN N-terminal region suggested that it might be susceptible to proteolysis. As an initial test of this hypothesis, we treated full-length SPIN with the relatively non-specific protease, subtilisin. Indeed, characterization of the reaction products by SDS-PAGE and MALDI-TOF mass spectrometry revealed that the ten N-terminal residues of SPIN were removed following a 30 min exposure to catalytic levels of enzyme (Fig. 4.6).

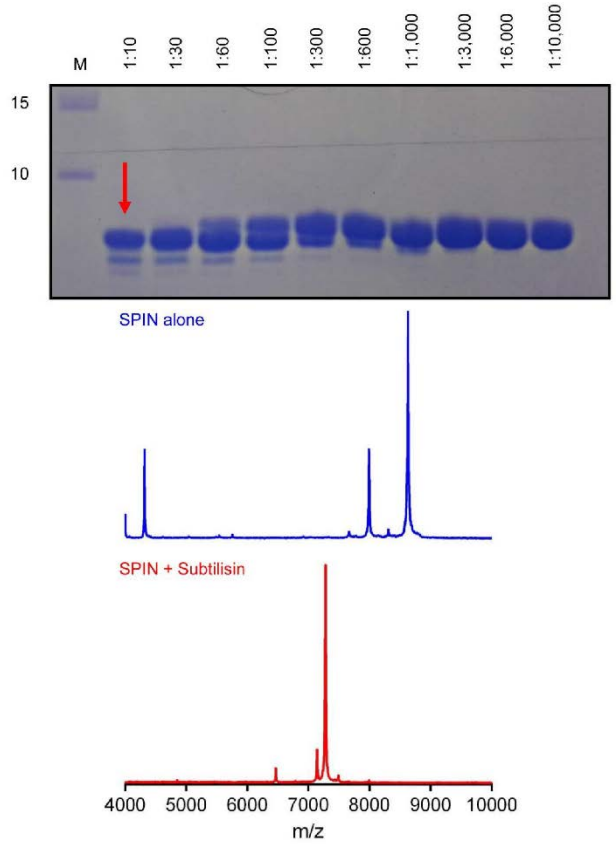

Figure 4.6 Limited Proteolysis of SPIN by Subtilisin. Full-length SPIN (1 µg/µl) was subjected to limited proteolysis by Subtilisin for 30 min at room temperature. Serial dilutions of protease mass relative to the SPIN substrate were prepared as indicated, and the digestion products were separated by 16% Tris-Tricine PAGE. Whereas full-length SPIN showed a major species (m/z = 8,629) that matched the expected mass of the recombinant protein, the protease stable digestion product (red arrow in the top panel; m/z = 7,280) corresponded to SPIN residues 43-105 (7,279 Da expected).

To examine the protease sensitivity of SPIN under more biologically relevant conditions, we tested whether the three canonical NSPs Neutrophil Elastase (NE), Cathepsin G (CG), and Proteinase-3 (PR3) might also degrade the SPIN N-terminus. Moreover, because this region of SPIN is required for SPIN to inhibit MPO (Fig.4.5), we investigated the functional consequences of such proteolysis using an MPO activity assay. We found that an excess of NE had to be incubated with SPIN to restore MPO activity to appreciable levels (Fig. 4.7A); this was due to incomplete cleavage by NE and residual full-length SPIN present in the reaction (Fig.4.8). By contrast, we observed that incubation of SPIN with either CG (Fig. 4.7B) or PR3 (Fig. 4.7C) each resulted in loss of MPO-inhibitory activity in a dose-dependent manner. Significantly, analysis of the SPIN cleavage products after CG and PR3 treatment not only showed clear evidence of proteolysis in the SPIN N-terminal region (Figs. 4.8 and 4.9), it was also consistent with the established cleavage preference for these NSPs [70].

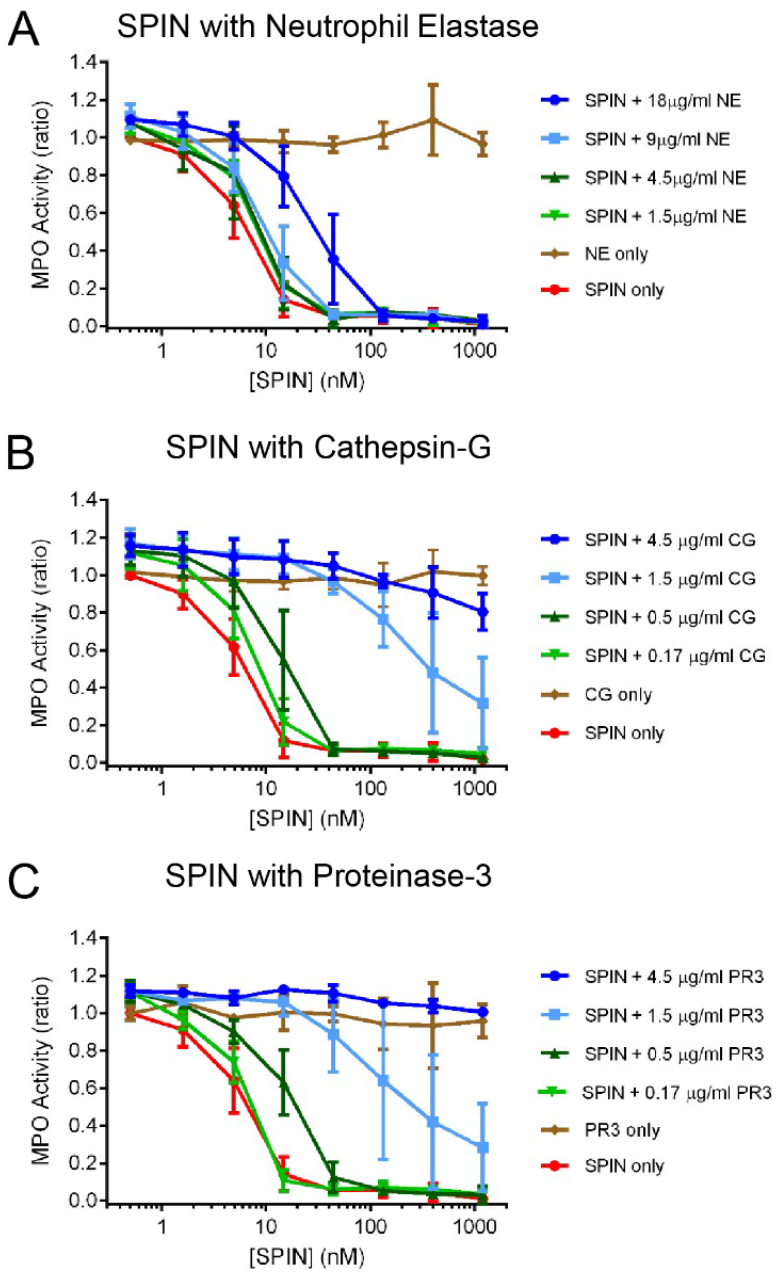

Figure 4.7 The N-terminal Region of SPIN is Subject to Proteolysis by NSPs. The influence of three proteases found in neutrophil azurophilic granules on SPIN activity was investigated using a spectrophotometric assay. Four different concentrations of (A) NE, (B) CG, and (C) PR3 were incubated with purified SPIN for 1 h after which proteolysis was stopped by adding PMSF. The reaction contents were serially diluted and incubated with MPO for 1 h further, prior to addition of a substrate mixture. Peroxidase activity was then measured at $OD_{450\ nm}$ relative to a negative control for each set of samples. Significantly, preincubation with all three NSPs examined resulted in dose-dependent loss of SPIN activity, although this effect was far more pronounced for CG and PR3 when compared to NE. Subsequent characterization of the NSP digestion products of SPIN revealed that loss of activity was due to specific cleavage of the functionally essential SPIN N-terminal region (Figs. 4.8-4.9). Bars express SD with N=3, and legends are inset.

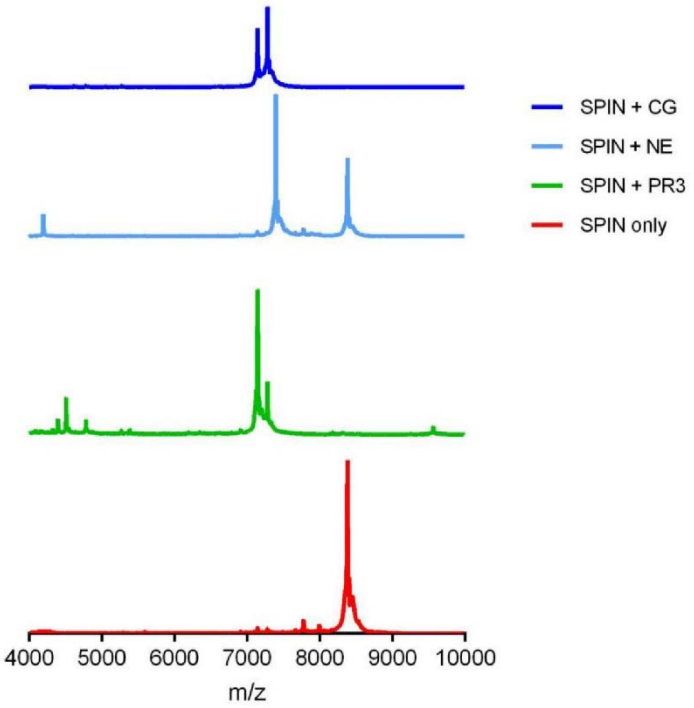

Figure 4.8 MALDI-TOF Spectra of SPIN Following Digestion with Various NSPs. Purified SPIN was incubated for 1 h with 18 µg/mL NE, 4.5 µg/mL CG, or 4.5 µg/mL PR3 after which proteolytic activity was stopped by addition of PMSF. A portion of the NSP-treated SPIN samples were assayed for their MPO-inhibitory activity (Fig. 4.7), while additional samples were examined for evidence of proteolytic digestion by MALDI-TOF mass spectrometry. Whereas the untreated SPIN protein showed no evidence of cleavage (m/z = 8,381), samples of SPIN treated with either CG (m/z = 7,278) or PR3 (m/z = 7,142) were characterized by well-defined smaller molecular weight species consistent with site-specific proteolysis. SPIN treated with NE appeared to result in incomplete digestion (m/z =7,392 and 8,381), however, which explained the residual MPO inhibitory activity found in this sample (Fig. 4.7A).

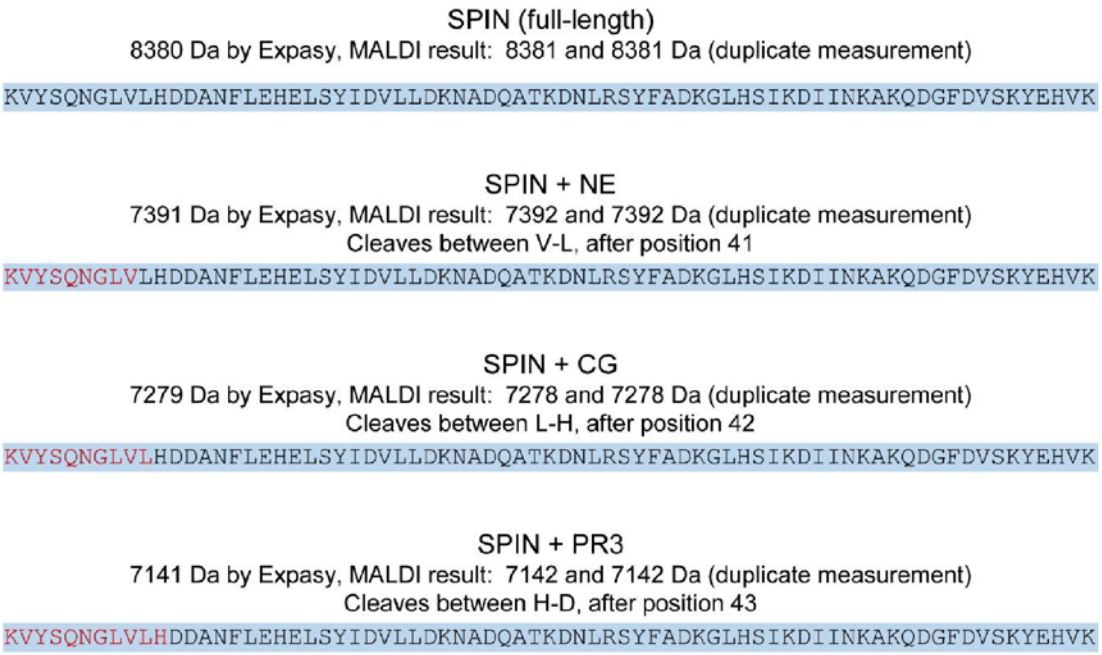

Figure 4.9 Further Characterization of SPIN Cleavage Products Following Proteolysis by NSPs. The MALDI-TOF data presented in Fig. 4.8 were compared to the sequence of SPIN to more fully characterize each digestion reaction. The main product of each SPIN digest was in good agreement with the known cleavage site preferences of NE, CG, and PR3. The identity of those residues removed upon digestion by each NSP is shown in red typeface. Together, these data indicate that the SPIN N-terminal region is cleaved by CG and PR3, and to a lesser extent, NE.

We previously showed that production of SPIN is upregulated following phagocytosis of *S. aureus* cells [1]. A similar increase in expression has also been reported for the genes encoding Eap and EapH1 upon exposure of *S. aureus* to crude neutrophil degranulate [71]. Since both Eap and EapH1 act as specific inhibitors of NSPs [26], we wondered whether these staphylococcal innate immune evasion proteins might rescue SPIN from deleterious proteolysis by NSPs. To test this possibility, we repeated the assays described above both in the absence and presence of saturating levels of recombinant Eap [26].

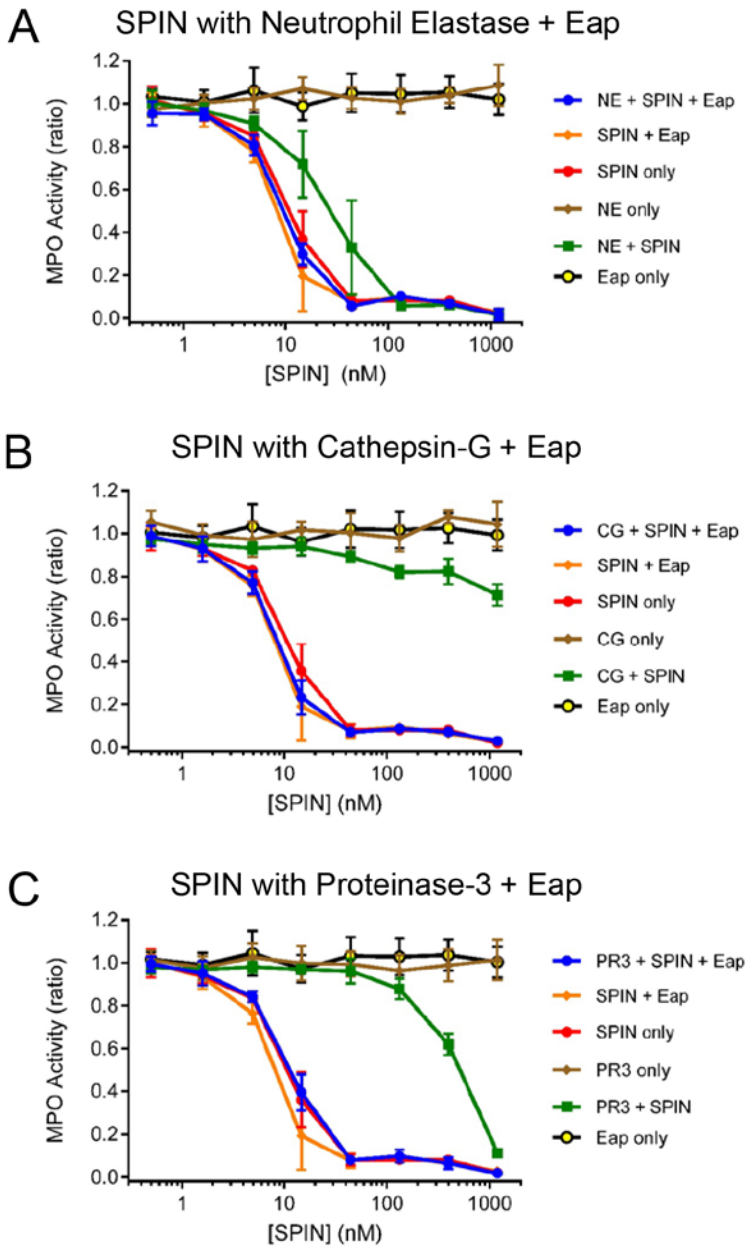

Figure 4.10 *S. aureus* Eap Protects the N-terminus of SPIN from Degradation by NSPs. The consequences of including the *S. aureus* derived NSP inhibitor, Eap [72], in the SPIN/NSP proteolysis reactions were assessed using an assay format identical to that presented in Fig. 4.7. The presence of Eap protected the N-terminus of SPIN from proteolysis by (A) 18 µg/mL NE, (B) 4.5 µg/mL CG, and (C) 4.5 µg/mL PR3. Importantly, while SPIN on its own inhibited MPO activity, the addition of Eap was required to fully-restore SPIN function in the presence the NSPs. Bars express SD with N=3, and legends are inset.

Consistent with the previously described NSP-inhibitory function of Eap [26], as well as prior results shown here (Fig. 4.7), we found that Eap protected SPIN from degradation by all three canonical NSPs (Fig. 4.10). Together, these results show that the N-terminal region of SPIN is subject to proteolysis by NSPs, but can be protected from such degradation through the action of the *S. aureus* NSP inhibitor, Eap.

Discussion

The last decade has witnessed tremendous growth in our understanding of staphylococcal innate immune evasion. In many respects, a majority of the functional, mechanistic, and structural details have been elucidated for those *S. aureus* secreted proteins that disrupt complement initiation and amplification, neutrophil recruitment, and the initial steps of phagocytosis [2, 17-19]. While the topic of intracellularly-acting immune evasion proteins has received considerably less attention, it is no less relevant; in fact, the ability of *S. aureus* cells to resist killing within the neutrophil phagosome suggests that additional evasion molecules remain to be undiscovered [2]. Recent work from our groups has led to identification of distinct *S. aureus* proteins that block function of NSPs [26] and MPO [1], which are key antimicrobial enzyme systems of neutrophils that act primarily within the phagosome [2, 6]. Herein, we have further defined the structure/function relationships of the novel MPO inhibitor, SPIN [1] (Figs. 4.2, 4.4-4.5). We have also provided evidence which suggests a potential functional synergy between SPIN and the EAP family of NSP inhibitors [26] (Figs. 4.7, 4.10). Together, this work significantly furthers our understanding of an only recently discovered aspect *S. aureus* immune escape.

Our previous crystal structure of SPIN/rMPO identified two MPO-binding sites within the SPIN protein [1]. While the relative contributions of each potential site to MPO binding could not be parsed directly from the structure, the biochemical data we present here have largely resolved this ambiguity. We found that loss of the SPIN N-terminal region has a minimal overall effect on its MPO-binding properties, as the K_D of 29.8 nM for $SPIN^{46-105}$/MPO compares favorably to that of 9.3 nM for SPIN/MPO (Fig. 4.4 and Table 4.1). Still, it is noteworthy that the observed 3.2-fold decrease in MPO affinity of $SPIN^{46-105}$ relative to its full-length counterpart is attributable almost entirely to a faster dissociation rate constant for its complex (3.7-fold enhancement (Table 4.1)). This result might be expected if the apparent interaction site involving the SPIN N-terminal region only forms after an initial binding event has occurred via the SPIN α-helical bundle. Consistent with this premise, synthetic peptides corresponding to both linear and constrained forms of the SPIN N- terminal region failed to bind MPO, even at concentrations some three orders of magnitude above the K_D for SPIN/MPO (Fig. 4.4 and Table 4.1). These data, along with a co-crystal structure of $SPIN^{46-105}$ bound to rMPO argue that the primary MPO-binding site of SPIN lies within its α-helical bundle domain.

Although the α-helical bundle is responsible for driving SPIN binding to MPO, we found that the SPIN N-terminal region is absolutely required for inhibiting MPO activity (Fig. 4.5). $SPIN^{46-105}$ binds MPO with relatively high affinity (Fig. 4.4 and Table 4.1), yet has no inhibitory capacity on its own (Fig. 4.5). This result appears to eliminate the possibility that SPIN binding inhibits MPO via perturbation of its heme redox chemistry, as has been described for the endogenous MPO inhibitor, ceruloplasmin [73]. In light of the data currently available, we favor a two-step steric/competitive model for SPIN action, whereby the initial MPO binding event is driven by the α-helical bundle region then the inhibitory β-hairpin folds and inserts into MPO

active site. In this manner, SPIN acts as a molecular plug, as suggested by our initial SPIN/rMPO crystal structure [1].

While deletion of the N-terminus yielded a SPIN protein that could not inhibit MPO, simply having these residues in the context of full-length SPIN was not sufficient to manifest inhibition on its own (Fig. 4.5). Our studies investigating residues His^{43}-Asp^{45} were particularly helpful in addressing this issue, as loss of these conserved sidechains caused only a 3.4-fold loss of affinity on MPO, yet rendered the $SPIN^{43\text{-}45\rightarrow AAA}$ mutant incapable of inhibiting MPO (Fig. 4.5). Examination of the SPIN/rMPO [1] structure reveals that both His^{43} and Asp^{44} form salt bridges with Asp^{379} and Arg^{271} of MPO, respectively. Since these residues do not seem to contribute significantly to MPO binding (Fig. 4.4 and Table 4.1), we suggest that His^{43}-Asp^{45} might help guide insertion of the inhibitory N-terminal β-hairpin into the MPO active site channel.

It seems that SPIN faces a rather precarious existence inside the phagosomal compartment. While SPIN is absolutely dependent on its N-terminus for function (Fig. 4.5), this region of the protein is dynamic in the absence of its binding partner (Fig. 4.2) and sensitive to proteolysis by NSPs in a manner that yields biologically inactive SPIN fragments (Figs. 4.7-4.9). Although the high concentration of MPO within the maturing phagosome would appear to promote stability of SPIN by effectively chaperoning its N-terminus, the abundance of NSPs in the same environment suggests that a significant portion of SPIN molecules could be cleaved soon after secretion. In light of this, our observation that *S. aureus* Eap preserves SPIN function by inhibiting CG, NE, and PR3 is a potentially significant finding. All three *S. aureus* EAP domain-containing proteins act as tightly binding, non-covalent inhibitors of NSPs [26], and they have been shown to protect against NSP-mediated cleavage of key staphylococcal virulence

factors in vitro and in vivo [74]. Although that previous study examined virulence proteins that act in the extracellular environment [74], our results here suggest that EAP domains can serve a similarly protective role for SPIN, and perhaps other molecules whose primary sites of action lie within the phagosomal compartment. While these results highlight the potential for functional synergy among various *S. aureus* immune evasion proteins, much work remains to be done if we are to truly understand the complex relationships of these proteins with one another. In this regard, long-standing evidence describing functional synergy between MPO and NSPs [13] serves as an important reminder that the numerous biochemical events inside the phagosome are best considered as part of an overall process, rather than reactions in isolation.

Chapter 5 - Identification and Structural Characterization of a Novel Myeloperoxidase Inhibitor from *Staphylococcus delphini*

Nicoleta T. Ploscariu[1], Nienke W.M. de Jong[2], Kok. P.M. van Kessel[2], Jos A.G. van Strijp[2], and Brian V. Geisbrecht[1, *]

[1]*Department of Biochemistry & Molecular Biophysics, Kansas State University Manhattan, KS, USA 66506*

[2]*Department of Medical Microbiology, University Medical Center Utrecht, Utrecht University, 3584 CX Utrecht, The Netherlands*

Although molecular level analysis of *S. aureus* SPIN (hereafter SPIN-*aureus*) has provided fundamental insights into the structure and function of this novel MPO inhibitor, our current understanding is restricted to sequence/structure features specific to the SPIN-*aureus* protein. To circumvent this limitation, we sought to identify SPIN-*aureus* homologs in other staphylococcal species and characterize their interactions with and effects on human MPO. We report here the identification of eight SPIN homologs, three of which bind to and inhibit human MPO in a dose-dependent manner. We also present a 2.4 Å co-crystal structure of SPIN from *Staphylococcus delphini* (SPIN-*delphini*) bound to rhMPO. This work not only allows the first comparative analyses of SPIN proteins, it also broadens our appreciation of a unique class of MPO inhibitor that functions in staphylococcal evasion of neutrophil-mediated immunity.

Identification of SPIN Homologs in a Subset of Staphylococcal Species

The *spn* gene is nearly ubiquitous among both human and animal-derived clonal lineages of *S. aureus* [1]. Furthermore, aside from *S. aureus* strains Mu3 and Mu50 which encode a substantially truncated and therefore inactive protein, there is little variability in the SPIN coding sequence between *S. aureus* strains [1]. Although these previous studies indicated that SPIN is highly conserved among *S. aureus* strains, we wondered whether genes encoding SPIN homologs might be found in related staphylococcal species. To test this possibility, we used the BLASTP algorithm to query the NCBI non-redundant protein database for any uncharacterized molecules with sequence homology to SPIN-*aureus* from strain Newman. Indeed, we identified eight such proteins from closely related staphylococcal species that are documented pathogens of humans, livestock, and/or domestic companion animals. Since SPIN is targeted for secretion from the bacterial cell via an N-terminal signal peptide, we used the SignalP server

(http://www.cbs.dtu.dk/services/SignalP/) to deduce the predicted matured sequences of the SPIN homologs [75]. We then compared these sequences to one another and with SPIN-*aureus* using a combination of CLUSTAL OMEGA [76] and MultAlin [77] (Table 5.1).

Table 5.1 Amino Acid Identities and Similarities Among the SPIN Sequences from Various Staphylococcal Species.

SPIN	*sciuri*	*aureus*	*Chromogenes*	*agnetis*	*hyicus*	*schleiferi*	*delphini*	*intermedius*	*pseudintermedius*
sciuri	100	52	54	64	59	56	62	63	63
aureus	38	100	70	73	64	77	80	79	73
chromogenes	35	48	100	85	84	74	77	73	73
agnetis	41	52	75	100	90	74	77	73	76
hyicus	38	46	69	85	100	67	70	69	71
schleiferi	29	56	61	59	51	100	91	81	83
delphini	33	53	58	54	48	69	100	86	90
intermedius	39	57	53	50	47	59	74	100	91
pseudintermedius	38	57	55	55	49	69	75	81	100

identity

similarity

We found agreement in our phylogenetic analysis of these novel SPIN-like sequences and previous analyses that identified relationships between these staphylococcal species [78] (Fig. 5.1A). For example, *S. hyicus* and *S. agnetis* belong to the same clade of staphylococci [79]. Comparison of SPIN-*hyicus* and SPIN-*agnetis* revealed less than 5 point accepted mutations (PAM) and ~85% sequence identity between these two proteins. A similar relationship was observed between *S. schleiferi* and established members of the *Staphylococcus intermedius* group (SIG) (i.e. *S. intermedius*, *S. pseudintermedius*, and *S. delphini*) [80]. SPIN sequences

within this cluster share no less than ~59% identity with one another (i.e. SPIN-*intermedius* v. SPIN-*schleiferi*), and also display the highest overall sequence identities with SPIN-*aureus* (~53-57%). By contrast, the distant phylogenetic relationship between *S. sciuri* and other staphylococci [81, 82] was also reflected in the relatively low sequence identity of SPIN-*sciuri* with the other SPIN sequences we analyzed here (~29-39% identity).

All published structure/function analyses thus far have been carried out using either natively-produced or recombinantly-expressed SPIN-*aureus* [1]. In this regard, the overall sequence identity of the matured homologs to SPIN-*aureus* varies between 38-57% (Fig 5.1A and Table 5.1). Surprisingly, examination of a multiple sequence alignment revealed that only 10 of 73 positions (~14%) are invariant across the nine sequences analyzed (Fig. 5.1B-C). Of these, only six residues (G^{39}, L^{42}, D^{44}, D^{45}, H^{51}, and Y^{75} per SPIN-*aureus* numbering) were found at the SPIN-*aureus*/rhMPO interface, as judged by the co-crystal structure [1]. Interestingly, four of these residues (G^{39}, L^{42}, D^{44}, and D^{45}) lie within the N-terminal region of the SPIN protein. Although this region of SPIN-*aureus* appears to make only minor contributions to SPIN binding of MPO, it is essential for inhibiting MPO enzymatic activity [43]. Thus, the relatively low level of absolute identity within the known MPO-binding site of SPIN suggested that valuable insights might be gained from further structure/function studies on these SPIN homologs.

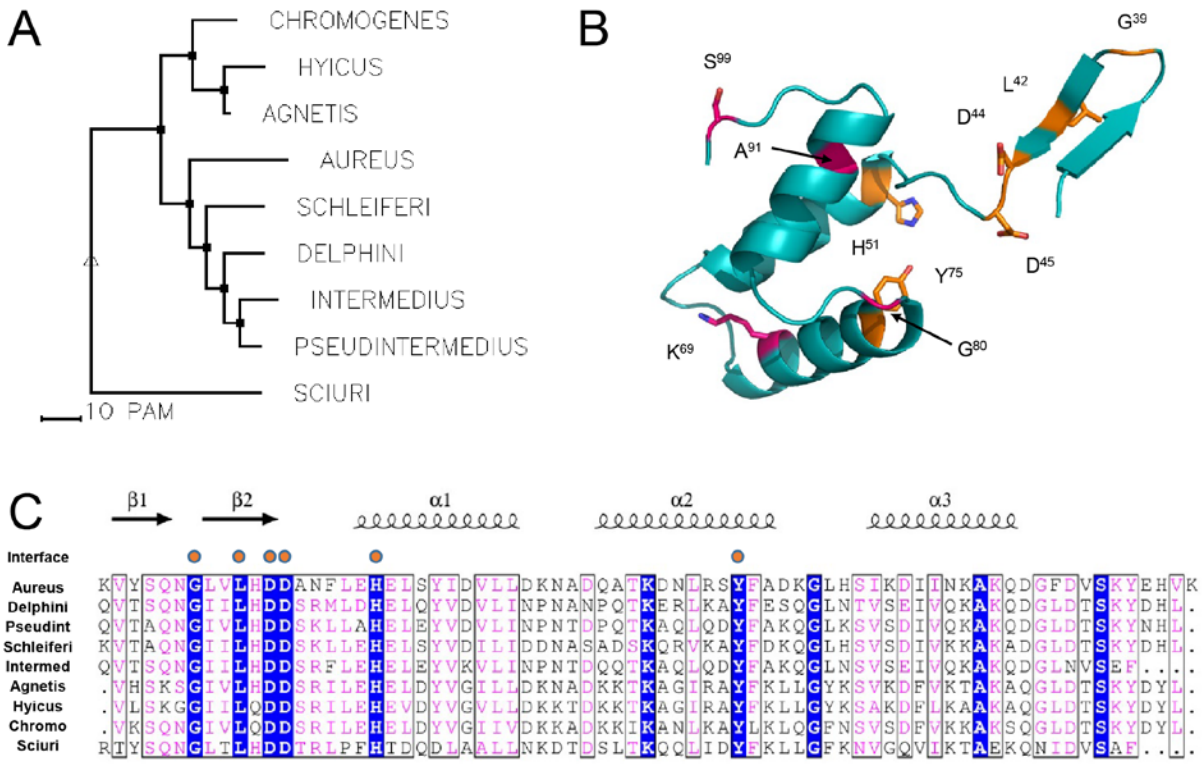

Figure 5.1 Analysis of Sequence Conservation Across Putative SPIN Homologs. A group of hypothetical sequences homologous to SPIN-*aureus* was identified by BLAST searching in the NCBI non-redundant protein database. The predicted mature form of each protein following cleavage of the signal peptide was determined via the SignalP server [75]. (A) Phylogenetic tree based upon the matured amino acid sequences of SPIN-*aureus* and eight other species of staphylococci. The tree is drawn to scale with branch lengths measured in the number of substitutions per site. (B) The structure of rhMPO-bound SPIN-*aureus* is shown as a ribbon diagram (PDB code 5UZU [1]). Residues invariant in all SPIN homologs and found at the SPIN/rhMPO interface are colored orange, while invariant residues that do not play a direct role in rhMPO contact are colored pink. Numbering reflects the sequence of matured SPIN-*aureus*. The N-terminal β-hairpin is shown at the top right of the image for purposes of orientation. (C) The sequences of putative SPIN homologs were aligned to that of SPIN-*aureus* using Clustal Omega [76], and displayed using EsPript [83]. Invariant residues are shown in reverse blue typeface, while residues conserved in a majority of sequences and conservative substitutions are shown in purple typeface. The secondary structure of rhMPO-bound SPIN-*aureus* is displayed above the alignment. Residues invariant across all SPIN homologs and found at the SPIN/rhMPO interface are designated with an orange circle.

A Subset of SPIN-aureus Homologs Bind to and Inhibit the Enzymatic Activity of Human MPO

Since genomic DNA was not readily available for all of these staphylococcal species, we designed synthetic coding sequences for each of the SPIN homologs, subcloned these fragments into a plasmid vector that directs expression of N-terminally His-tagged fusion proteins [35], and used these plasmids to produce highly purified forms of each putative SPIN. The integrity of each protein was confirmed by MALDI-TOF mass spectrometry. Unfortunately, the SPIN-*hyicus* protein appeared prone to degradation, and was thereby excluded from further analysis. We then examined the ability of each remaining SPIN protein to bind immobilized native human MPO by a surface plasmon resonance (SPR) approach. Injections of an increasing concentration of each recombinant SPIN gave clear evidence of binding for several of the homologs (Fig. 5.2). SPIN-*chromogenes* and SPIN-*sciuri* appeared to bind human MPO much more weakly than the others and were not analyzed further (*Data Not Shown*), while SPIN-*pseudintermedius* gave no evidence of binding whatsoever (Fig. 5.2). The reference subtracted sensorgrams for all other series were analyzed using a kinetic model of 1:1 binding to derive association (k_a), dissociation (k_d), and affinity constants (K_D) for each interaction (Table 5.2).

Table 5.2 Binding Analysis of SPIN Homologs to Native Human MPO as Determined by SPR* and IC_{50} Values as Determined from MPO Activity Assay.**

SPIN	k_a ($M^{-1}s^{-1}$) x 10^4	k_d (s^{-1}) x 10^{-3}	K_D (nM)	IC_{50} (nM)
aureus	20.10 ± 2.22	3.16 ± 0.04	15.9 ± 2.1	4.6 (2.7 - 7.8)
agnetis	5.64 ± 0.14	2.36 ± 0.10	41.8 ± 1.1	-
schleiferi	1.12 ± 0.14	2.52 ± 0.17	230 ± 42.1	261.2 (153.5 - 444.2)
delphini	1.08 ± 0.08	3.34 ± 0.17	310 ± 42.5	29.7 (23.0 - 51.4)
intermedius	0.35 ± 0.08	3.34 ± 0.12	984 ± 274	221.7 (159.1 - 308.9)

*Values represent the mean plus or minus the standard deviation obtained from replicate injections across three independent flow cells derivatized with native human MPO.
** Values represent the best fit value obtained from three replicate experiments with the 95% confidence interval provided in parenthesis.

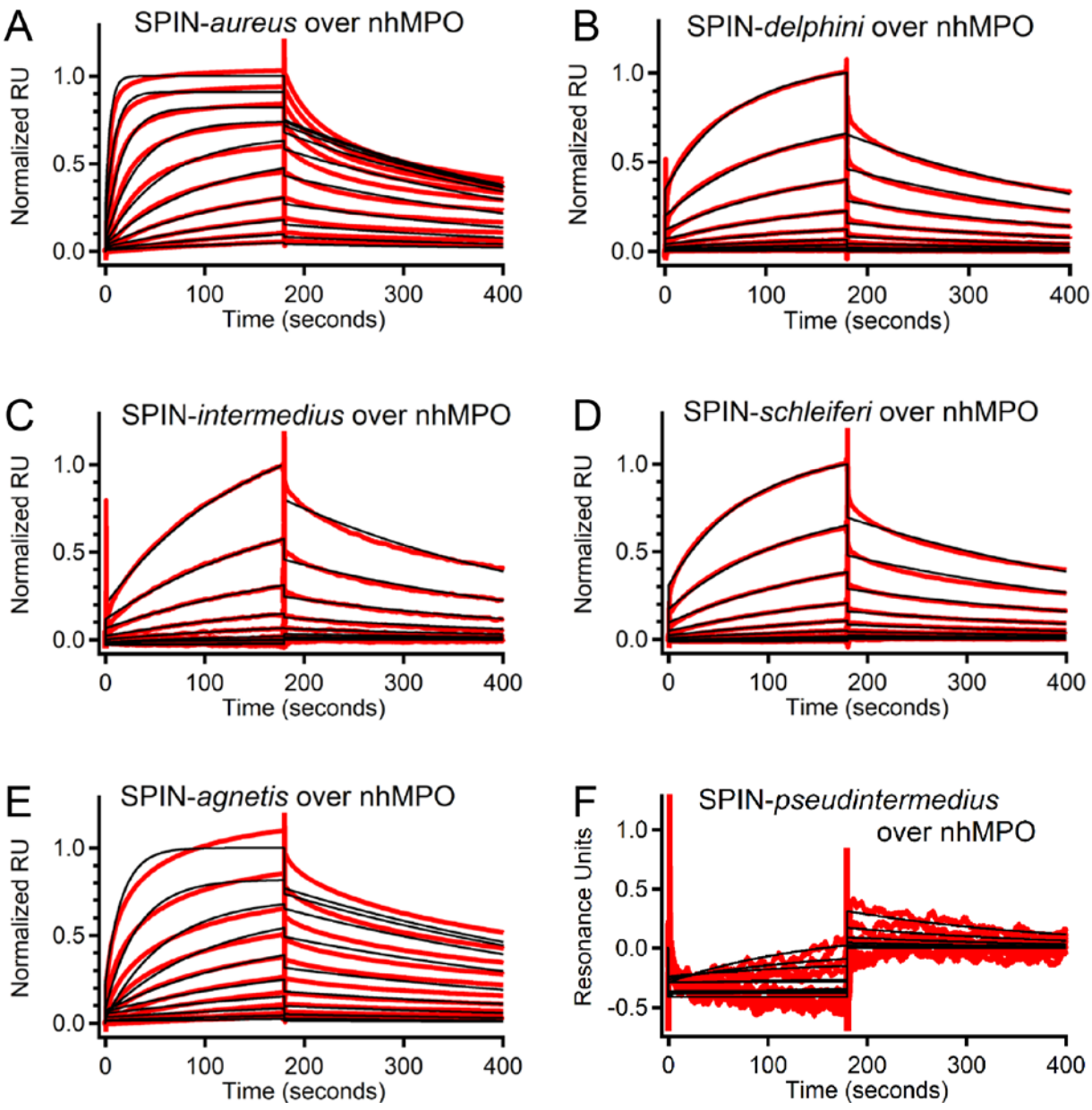

Figure 5.2 Characterization of SPIN Homolog Binding to Native Human MPO by Surface Plasmon Resonance. A two-fold dilution series of recombinant SPIN-*aureus* and various homologs was injected over three separate flow-cells of native human MPO that had been randomly immobilized at different surface densities. The reference-subtracted sensorgrams for each injection series (black traces) were fit to a 1:1 binding model (red traces) and normalized to their respective maximal responses. Representative sensorgram series are shown for native MPO binding to (A) SPIN-*aureus*, (B) SPIN-*delphini*, (C) SPIN-*intermedius*, (D) SPIN-*schleiferi*, and (E) SPIN-*agnetis*. (F) Representative traces for injections of SPIN-*pseudintermedius* over native MPO surfaces. SPIN-*pseudintermedius* does not appear to bind significantly to native human MPO, since the observed response values were very low for this homolog. As a consequence, the data were not normalized. Comparatively weak binding to human MPO was observed for SPIN-*chromogenes* and SPIN-*sciuri*, so these are not presented here in the interest of space.

We previously reported that SPIN-*aureus* binds immobilized native human MPO with an apparent K_D of 10±0.6 nM [1]. Replicate measurements performed during this present study yielded a similar value of 15.9±2.1 nM (Table 5.2), which indicated a high level of precision for the SPR interaction assay across several independent experiments. We found considerable variability in the interactions between human MPO and the SPIN homologs, however (Fig 5.2 and Table 5.2). Although no SPIN homolog bound MPO as well as SPIN-*aureus*, SPIN-*agnetis* displayed the second highest affinity for MPO, as judged by its K_D of 41.8±1.1 nM. The affinity of the remaining homologs ranged from 230±42.1 nM for SPIN-*schleiferi* to 984±274 nM for SPIN-*intermedius*. These values represent approximately 14.5 and 61.9-fold decreases in affinity for human MPO, respectively, when compared to SPIN-*aureus*. We also noted that all of the SPIN homologs that bind human MPO had similar dissociation rate constants (k_d), which ranged from $2.36x10^{-3}$ to $3.34x10^{-3}$ s^{-1} as a group. Conversely, the association rate constants (k_a) for binding to MPO varied widely, from a high of $20.1x10^4$ $M^{-1}s^{-1}$ for SPIN-*aureus* to a low of $0.354x10^4$ $M^{-1}s^{-1}$ for SPIN-*intermedius*. Thus, nearly all of the differences in affinity for human MPO displayed by these SPIN homologs are attributable to variations in their association rate constants.

Our co-crystal structure of SPIN-*aureus*/rhMPO indicates that SPIN acts as a molecular plug to block solute exchange to and from the MPO active site [1]. However, subsequent studies on a series of site-directed and deletion mutants of SPIN-*aureus* revealed that binding to MPO is necessary, but not sufficient for inhibiting its activity [43]. We therefore sought additional information on whether the SPIN homologs that bound MPO in the SPR assay could also block MPO function in an enzymatic activity assay. We used a colorimetric activity assay to examine the ability of each SPIN to inhibit MPO function *in vitro* (Fig 5.3). Each SPIN homolog was

added to the assay in triplicate across a dilution series that spanned three orders of magnitude. Consistent with our previous work, we found that SPIN-*aureus* significantly inhibited MPO activity under these conditions (IC_{50} ~8 nM)[1, 43]. Conversely, we also found that all SPIN variants that failed to bind human MPO (i.e. SPIN-*sciuri*, SPIN-*chromogenes*, and SPIN-*pseudintermedius*) also failed to inhibit its activity.

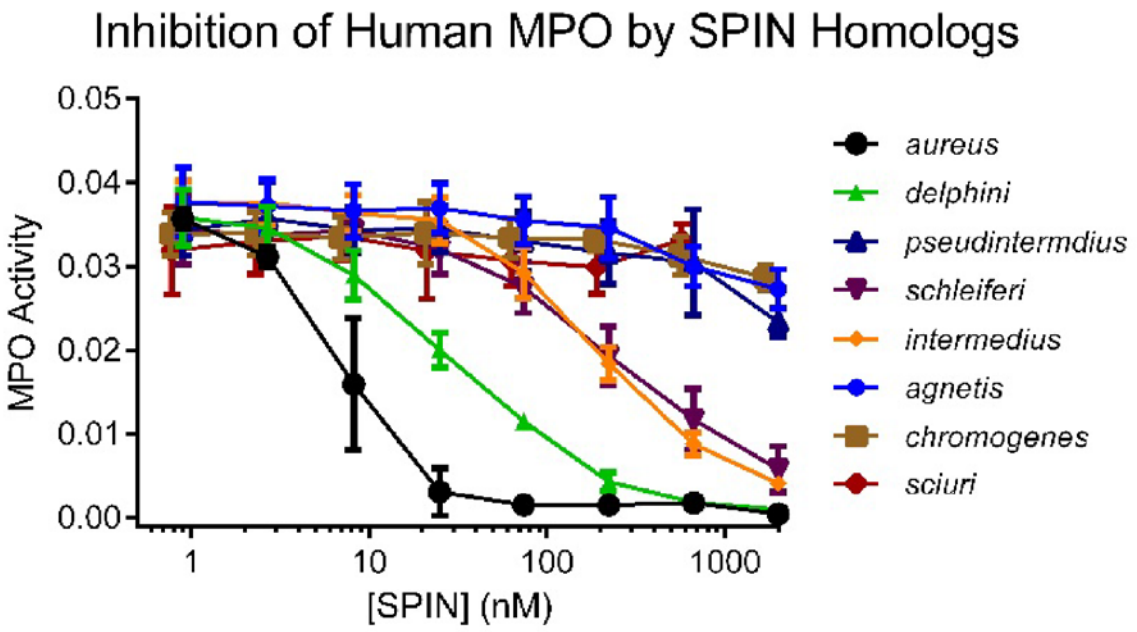

Figure 5.3 . A Subset of SPIN Homologs Inhibit the Enzymatic Activity of Native Human MPO. The enzymatic activity of native human MPO was investigated across a dilution series of various recombinant SPIN homologs. Initial reaction velocities were determined in triplicate at each concentration point prior to curve fitting and determination of IC_{50} values. Whereas SPIN-*delphini*, SPIN-*schleiferi* and SPIN-*intermedius* all inhibit MPO in a dose-dependent manner, SPIN-*agnetis* fails to do so even though it binds with low-nanomolar affinity to native MPO. SPIN-*aureus* is included as a control for inhibition [84]. Bars express the mean plus or minus the standard deviation (n=3). A legend is inset.

Out of the homologs that remained, we found that three retained a clear inhibitory capacity against human MPO. Whereas SPIN-*intermedius* and SPIN-*schleiferi* inhibited MPO with IC_{50} values of ~200 nM, SPIN-*delphini* displayed an approximately 6.7-fold more potent IC_{50} value of ~30 nM. These differences in IC_{50} values were somewhat unexpected, given that these three SPIN homologs are part of the same phylogenetic clade and share over 60% identity with one another (Fig. 5.1A and Table 5.1). The most surprising results were obtained for SPIN-*agnetis*. This protein failed to significantly inhibit MPO at concentrations up to 2 μM, even though it binds human MPO with a K_D of 41.8 nM as judged by SPR (Fig. 5.2 and Table 5.2). In this regard, the functional properties of SPIN-*agnetis* most closely resemble those of a site-directed mutant in SPIN-*aureus* where the conserved sidechains of H^{43}, D^{44}, and D^{45} were simultaneously changed to alanine [43]. This mutant also failed to inhibit MPO despite the fact that it binds MPO with a K_D near 30 nM.

The Crystal Structure of SPIN-delphini Bound to Recombinant Human MPO at 2.4 Å Resolution

We required additional structural information on rhMPO in complex with a tightly binding SPIN homolog in order to better understand the similarities and differences among these newly identified SPIN family members. We succeeded in growing single crystals of SPIN-*delphini* bound to rhMPO that diffracted synchrotron X-rays to 2.4 Å limiting resolution and solved and refined this structure to R_{work}/R_{free} values of 18.5 and 21.8%, respectively (Fig. 5.4A and Table 5.3). As expected, the structure of SPIN-*delphini*/rhMPO compares favorably to the structure of SPIN-*aureus*/rhMPO (Fig. 5.4B), as the 539 Cα positions from the two coordinate sets that align with one another superimpose with an RMSD of 0.289 Å. When we compared

only the structures of rhMPO-bound SPIN-*aureus* and SPIN-*delphini* to one another, the 61 Cα positions align with an RMSD of 0.812 Å (Fig. 5.4C). This high level of structural identity was preserved throughout the entirety of the models, save for some minor deviations at the proteins' N and C-termini.

For reasons that remain unclear, our crystal structures of rhMPO bound to either full-length or an N-terminally deleted SPIN-*aureus* are characterized by low occupancy of the heme prosthetic group [43, 84]. Absence of the heme was not required for SPIN binding though, as full-length and N-terminally deleted SPIN-*aureus* bind equally well to both rhMPO and native MPO that had been isolated from purulent human sputum [43, 84]. Interestingly, examination of the F_o-F_c electron density map calculated after initial placement of the polypeptide models in the SPIN-*delphini*/rhMPO asymmetric unit revealed an obvious planar density at contour levels up to 3σ within the rhMPO active site (Fig. 5.4D). Following model building and refinement, our final SPIN-*delphini*/rhMPO coordinates have full occupancy of the heme prosthetic group with a median B-factor of 57.6 $Å^2$. This value is consistent with the structure as a whole, whose all atom mean B-factor is 56.8 $Å^2$ (Table 5.3).

Table 5.3 X-ray Diffraction Data Collection and Refinement

	SPIN-*delphini*/rhMPO
Data Collection	
Space group	*P* 2_1 2_1 2_1
Cell dimensions	
a, *b*, *c* (Å)	84.63, 90.67, 125.66
Resolution (Å)	45.34-2.40 (2.49-2.40)*
R_{pim}	0.045 (0.382)
$I / \sigma I$	15.5 (1.7)
Completeness (%)	99.7 (97.2)
Redundancy	13.5 (7.7)
Refinement	
Resolution (Å)	45.34-2.40
Number of Reflections	36,188
R_{work} / R_{free}	18.5/21.8
No. atoms	
Protein	5143
Ligand/ion	87
Solvent	105
Mean *B*-factors (Å^2)	
Protein	56.8
Ligand/ion	65.3
Solvent	50.9
R.M.S. deviations	
Bond lengths (Å)	0.015
Bond angles (°)	1.48
PDB accession code	6BMT

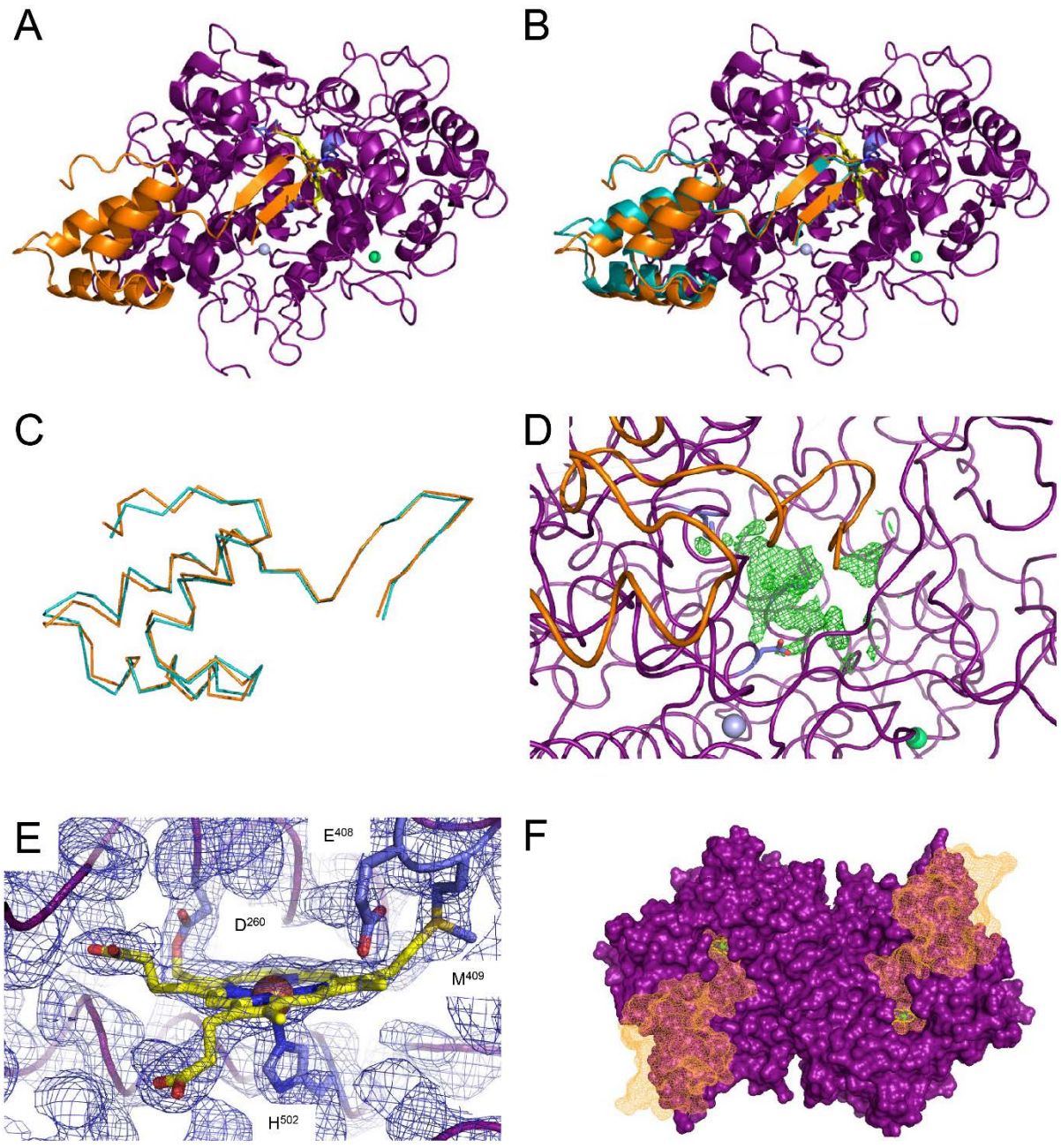

Figure 5.4 The Structural Basis for Inhibition of MPO by SPIN-*delphini*. (A) A 2.4 Å co-crystal structure of rhMPO (purple) bound to SPIN-*delphini* (orange). Proteins are represented as ribbon diagrams, while the covalently bound heme prosthetic group is drawn in ball-and-stick convention with carbon atoms in yellow, nitrogen in blue, oxygen in red, and the iron ion as a red sphere. Ordered Ca^{2+} and Cl^- ions are drawn as light blue and green spheres, respectively. (B) Superposition of the SPIN-*aureus*/rhMPO co-crystal structure (PDB code 5UZU [84]) onto the SPIN-*delphini*/rhMPO structure as shown in panel A. SPIN-*aureus* is drawn as a cyan ribbon. (C) Superposition of rhMPO-bound forms of SPIN-*aureus* (cyan) and SPIN-*delphini* (orange). The proteins are drawn in wire convention with the N-terminal β-hairpin at the right-hand side of the image. (D) F_o-F_c electron density map (green mesh contoured at 2.5σ) within the rhMPO active site after initial structure solution by molecular replacement.

The proteins chains are colored identically to the panels above for clarity, while the locations of the Ca^{2+} and Cl^- ions are included for reference. (E) Properties of the heme prosthetic group in the final model of SPIN-*delphini*/rhMPO. The heme is drawn as in panel A, while noteworthy rhMPO sidechains (labels insert) are drawn as stick models (carbon atoms light purple). Note the inclusion of three covalent bonds as described in the text. $2F_o$-F_c electron density (blue mesh contoured at 1.3σ) is shown as an indicator of model to map correlation. (F) Visualization of the SPIN binding site on MPO in the context of the native human MPO dimer. Two copies of the SPIN-*delphini*/rhMPO structure were superimposed on native human MPO (PDB code 1CXP [85]). MPO is drawn in purple as a molecular surface, while SPIN-*delphini* is drawn as an orange, space-filling mesh. The heme is drawn as in panel A, with the exception that the iron ion is colored green to enhance contrast.

The final $2F_o$-F_c electron density maps were consistent with the existence of four covalent bonds between SPIN-*delphini* bound rhMPO and the heme group (Fig. 5.4E). However, we included only three of these four covalent bonds in our final model: H^{502} to heme Fe at 2.51 Å, M^{409} to heme CBB at 1.95 Å, and D^{260} to heme CMD at 1.58 Å. The final covalent bond between E^{408} and heme CMB was visible as contiguous density within the $2F_o$-F_c map at levels up to 1.4 σ, but at 2.16 Å fell outside an acceptable bond length for this linkage (c.f. 1.55 Å for the corresponding bond in PDB entry 1CXP [85]). We believe this discrepancy likely resulted from the lower positional certainty of coordinates at 2.4 Å resolution when compared to higher resolution structures, such as the 1.8 Å resolution structure of halide-bound native human MPO referenced above [85]. These minor differences aside, the structure of SPIN-*delphini*/rhMPO presented here demonstrates that binding of SPIN family proteins is not mutually exclusive with high occupancy of the heme prosthetic group in rhMPO.

Native MPO exists as a ~150 kDa dimer comprised of two heavy and two light chains, respectively [43]. Moreover, crystal structures of native MPO from both human [85] and canine [86] sources revealed the presence of dimers within the asymmetric unit. The crystals of SPIN-*aureus* bound to rhMPO contain only a single copy of each polypeptide in the asymmetric unit [84], however, and examination of the protein-protein interfaces created by crystallographic

symmetry operators showed no dimeric features equivalent to those found in native MPO. Similarly, the crystals of SPIN-*delphini*/rhMPO likewise contain only a single copy of the complex within the asymmetric unit (Fig. 5.4A), and there was no dimer equivalent to native MPO visible via crystallographic symmetry operations. Despite the fact that both SPIN-*aureus* and SPIN-*delphini* crystallized with rhMPO as binary complexes, we found that each of these structures is still compatible with the dimeric assembly found in native MPO (Fig. 5.4F). Superposition of both sets of coordinates onto the structure of dimeric native MPO revealed no obvious steric clashes that would prevent binding of either SPIN to such an arrangement. In fact, this is consistent with analytical gel filtration chromatography studies that show clear evidence for binding of SPIN-*aureus* to native human MPO (Fig. 5.5). Thus, the differences in oligomerization state observed in our structural studies most likely resulted from the rhMPO we used in this work, rather than reflecting *bona fide* consequences of SPIN binding to MPO.

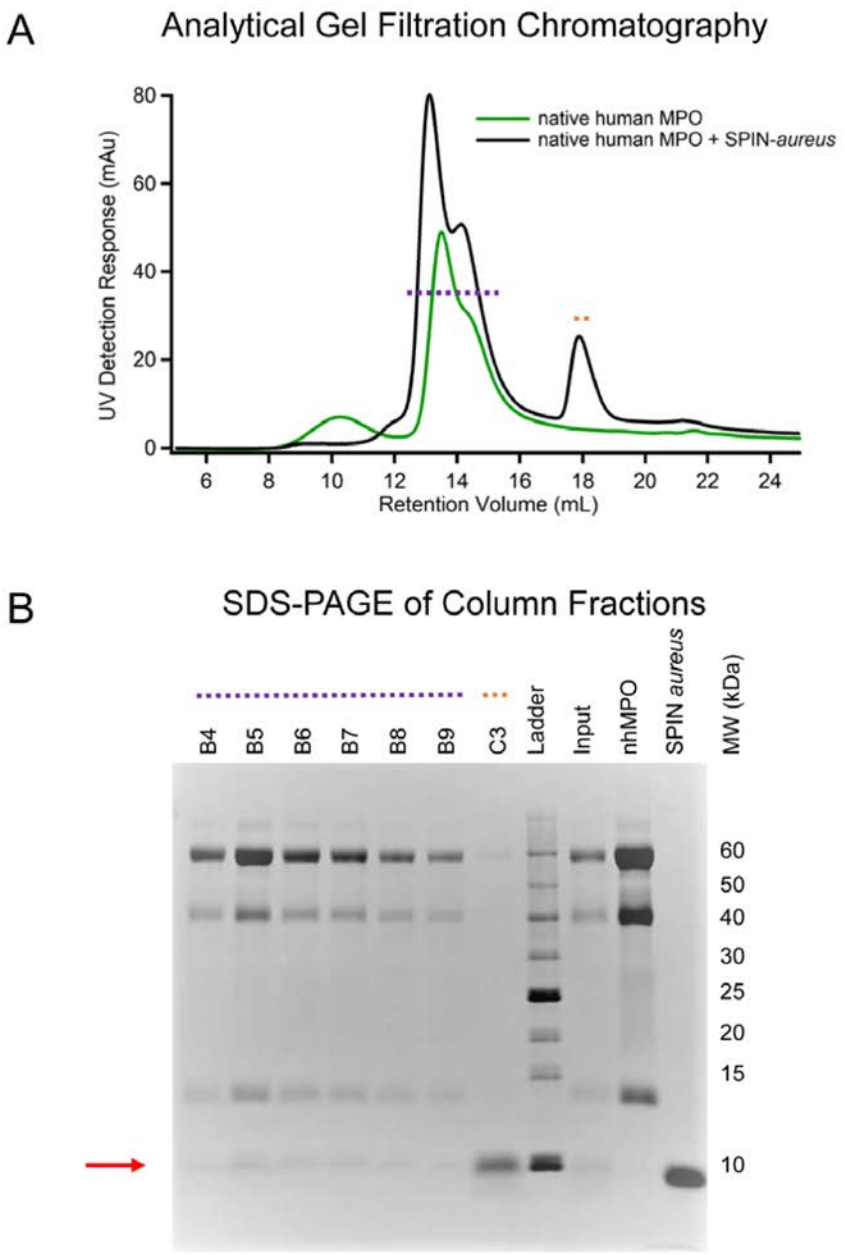

Figure 5.5 Co-purification of SPIN-*aureus* with Native Human MPO. Samples of either native human MPO (nhMPO) alone or in the presence of a stoichiometric excess of SPIN-*aureus* were separated by analytical gel filtration chromatography using a Superdex S200 10/30 column (GE Healthcare). (A) Representative chromatograms for either nhMPO alone (green trace) or nhMPO + SPIN-*aureus* (black trace). The peak of the nhMPO + SPIN-*aureus* sample corresponds to an observed molecular weight of ~120 kDa, as judged by comparison to calibration standards. (B) SDS-PAGE analysis of various column fractions in comparison to the starting material (input) and various controls (labeled). Individual fractions from the nhMPO + SPIN-*aureus* sample spanning the regions corresponding to either the dashed purple or orange line are shown. The presence of SPIN-*aureus* is designated with a red arrow.

Sequence-Dependent Structural Differences Between SPIN-delphini and SPIN-aureus Offer an Explanation for Their Differences in Affinity for Human MPO

Whereas SPIN-*delphini* and SPIN-*aureus* form complexes with rhMPO that closely resemble one another (Fig. 4B), the affinities of these proteins for MPO differ by nearly 20-fold at 310 nM and 15.9 nM, respectively (Table 1). Since SPIN-*delphini* shares 53% identity with SPIN-*aureus*, we considered whether the differences in affinities observed by SPR were due to alterations of key sidechains found at the SPIN/rhMPO interfaces. We analyzed the SPIN-*delphini*/rhMPO complex using the PISA server [87] and used the output to construct both an interface map (Fig. 5.6A) and a list of likely intermolecular interactions (Table 5.4). We then compared these data from SPIN-*delphini*/rhMPO to analogous results obtained for SPIN-*aureus*/rhMPO [84] (Table 5.4).

We determined that the total number of inhibitor-derived residues at the SPIN-*delphini*/rhMPO interface (30) is nearly identical to that of SPIN-*aureus*/rhMPO (31) (Fig. 5.6A-B). Consistent with the overall identity between these two proteins, however, only 17 interfacing residues are identical between SPIN-*delphini* and SPIN-*aureus*. Given that even minor changes at the interface might result in altered surface compatibility between rhMPO and the two SPINs, we analyzed the surface complementarity of both structures using the program s.c. [88]. Both SPIN-*delphini*/rhMPO and SPIN-*aureus*/rhMPO have similar overall s.c. coefficients of 0.715 and 0.704, respectively; these values are slightly lower than those of other high-affinity protein/protein interactions relevant to staphylococcal innate immune evasion, such as that of the neutrophil serine protease inhibitor, EapH1, bound to neutrophil elastase (s.c. = 0.77) [72].

Table 5.4 Comparative Interface Analysis of SPIN-*delphini*/rhMPO and SPIN-*aureus*/rhMPO.

SPIN-*delphini*	Bond type	SPIN-*aureus*	Bond type	MPO residue
		33 LYS	HS	GLU346
29 VAL		34 **VAL**		
30 THR		35 TYR	H	GLU346
31 SER	H	36 **SER**	H	GLU268
32 GLN	H	37 **GLN**		THR265
33 ASN	H	38 **ASN**	H	GLU268
34 GLY		39 **GLY**		
35 ILE		40 LEU		
36 ILE		41 VAL		
37 LEU		42 **LEU**		
38 HIS	S	43 **HIS**	HS	ASP380
39 ASP		44 **ASP**	HS*	ARG272*
40 ASP		45 **ASP**	H	ASN352
42 ARG	H	47 ASN	H	ASN381
		47 ASN	H	HIS383
43 MET	H	48 PHE	H	ASN381
44 LEU		49 **LEU**		
45 ASP	S	50 GLU	HS	ARG368
46 HIS	H	51 **HIS**	H	ASN352
47 GLU				
49 GLN		54 SER		
50 TYR	H	55 **TYR**	H	MET356
		55 **TYR**	H	ARG354
53 VAL		58 **VAL**		
62 GLN				
63 THR		68 **THR**		
66 ARG		71 ASN		
67 LEU		72 **LEU**		
70 TYR	H	75 **TYR**	H	ASN352
		78 ASP		
74 GLN		79 LYS	H	ASN352
		93 GLN		
89 ASP	H	94 **ASP**	H	ASN381
		95 GLY		
91 LEU		96 PHE		
92 ASP				

Identical Positions in Bold Typeface
H: hydrogen bond
S: salt bridge
***ARG272 is found on apo-MPO only**

residues at the interface with MPO
bond forming residues, only by SPIN-*delphini*
bond forming residues, only by SPIN-*aureus*
bond forming residues, by both SPIN proteins

Nevertheless, since previous work had shown that the SPIN-*aureus*/MPO interaction primarily arises via the α-helical bundle region of the inhibitor [43], we recalculated the s.c. coefficients of these structures in the absence of the N-terminal β-hairpin motifs. This yielded an s.c. value of 0.715 for SPIN-*delphini*/rhMPO, but of 0.774 for SPIN-*aureus*/rhMPO. We considered the rather large difference between these two s.c. values as evidence that the α-helical bundle region SPIN-*aureus* is far better suited to packing tightly against rhMPO than is SPIN-*delphini*. Consistent with this prediction, SPIN-*delphini* buries only 1365 $Å^2$ of its surface area when bound to rhMPO. This value is only ~85% of that previously reported for SPIN-*aureus* [84].

We also found that the number of polar interactions (i.e. hydrogen bonds and salt bridges) formed with rhMPO is considerably smaller for SPIN-*delphini* than for SPIN-*aureus*. Of the 31 residues found at the interface between SPIN-*aureus* and rhMPO, 14 appeared to participate in one or more polar contacts with groups from rhMPO. By contrast, of the 30 residues found at the SPIN-*delphini*/rhMPO interface, only 11 were judged to form polar contacts with rhMPO. Whereas seven of these residues are identical between the two SPINs and deemed to form equivalent interactions (i.e. S^{31}, N^{33}, H^{38}, H^{46}, Y^{50}, Y^{70}, and D^{89} per SPIN-*delphini* numbering), the other conserved position (i.e. D^{40}) fails to form a hydrogen bond in the SPIN-*delphini*/rhMPO structure even though it does so in the SPIN-*aureus*/rhMPO structure. Furthermore, three other positions in SPIN-*delphini* (i.e. Q^{28}, T^{30}, and Q^{74}) represent non-conservative changes when compared to SPIN-*aureus* and thereby disrupt polar contacts. Since only the Q^{74} from SPIN-*delphini* resides in the α-helical bundle, we surmised that this change from K^{79} in SPIN-*aureus* is likely the most significant alteration in terms of MPO binding. In that regard, we noted that the residues D^{45}, H^{51}, and K^{79} of SPIN-*aureus*

(corresponding to SPIN-*delphini* D^{40}, H^{46}, and Q^{74}) are all involved in hydrogen bonding to groups from position N^{352} of rhMPO (Fig. 5.6C-D). In the case of SPIN-*aureus* D^{45} versus SPIN-*delphini* D^{40}, the observed distance between acceptor and donor is 3.7 Å in SPIN-*aureus*/rhMPO compared to 4.2 Å in SPIN-*delphini*/rhMPO. A similar situation is found for SPIN-*aureus* K^{79} versus SPIN-*delphini* Q^{74}, where the observed distance to the N^{352} sidechain is 3.2 Å compared to 5.6 Å. Although both SPIN-*aureus* and SPIN-*delphini* utilize a conserved histidine sidechain (i.e. H^{51} and H^{46}, respectively) to form hydrogen bonds of ~3.0 Å distance to the backbone oxygen from N^{352} in rhMPO, disruption of the other interactions with the N^{352} sidechain as described above may be a contributing factor to the reduced affinity of SPIN-*delphini* for MPO.

In summary, while SPIN-*delphini* maintains an ability to bind human MPO and inhibit its activity (Figs. 2-3), the quantitative differences between SPIN-*delphini* and SPIN-*aureus* vis-à-vis affinity for and inhibition of MPO appear to be predicated on sequence/structure changes that affect both the overall shape and positioning of functional groups at the MPO binding site of these closely related proteins (Fig. 5.6E).

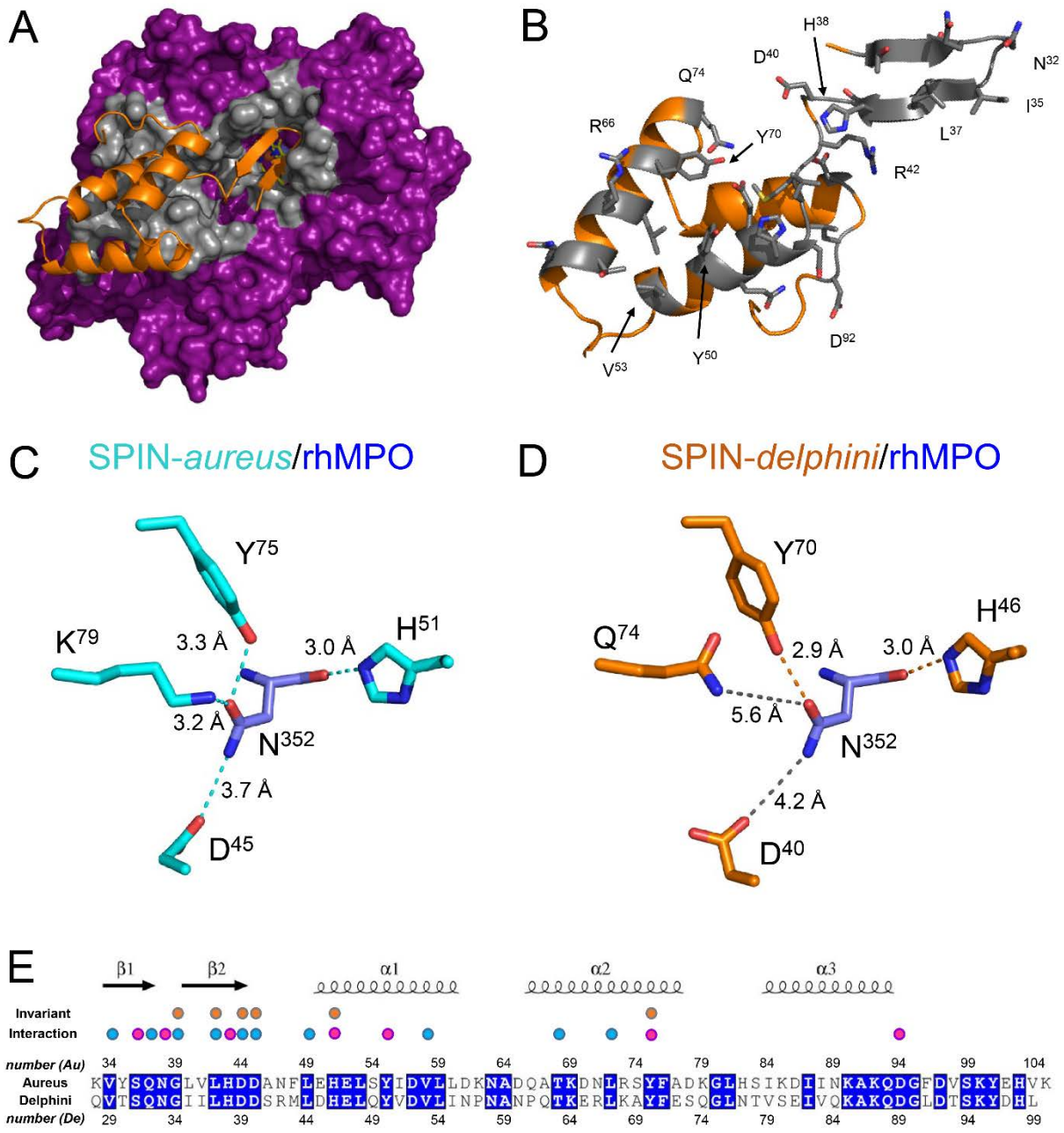

Figure 5.6 . Molecular Analysis of the SPIN-*delphini*/rhMPO Interface and Comparsion with SPIN-*aureus*/rhMPO. (A) Representation of the SPIN-*delphini*/rhMPO structure highlighting the residues comprising the SPIN-*delphini* binding site on rhMPO. SPIN-*delphini* is shown as an orange ribbon, while rhMPO is drawn as a molecular surface with non-interacting residues in purple and interfacing residues in grey. The heme prosthetic group is drawn as in Fig. 5.4 for reference. (B) The structure of SPIN-*delphini* drawn as an orange ribbon. Sidechains found at the rhMPO interface are drawn in stick convention with the carbon atoms colored grey. Selected sidechains are individually labeled. Note that this representation of SPIN-*delphini* is rotated approximately 180° in the plane of the page relative to panel A. (C) Polar interactions between SPIN-*aureu*s sidechains (cyan) and N^{352} of rhMPO (blue). Likely interactions (cyan dashes) and their corresponding distances are labeled. (D) Polar interactions between SPIN-*delphini* sidechains (orange) and N^{352} of rhMPO (blue). Likely interactions

(orange dashes) and their corresponding distances are labeled. Grey dashes represent interactions not formed due to excessive distance between donor and acceptor groups. (E) Sequence comparison between SPIN-*aureus* (numbering above) and SPIN-*delphini* (numbering below) with identical residues shown reverse blue typeface. The secondary structure of rhMPO-bound SPIN-*aureus* is displayed above the alignment. Identical residues found at the rhMPO interface of each complex that form non-polar interactions are indicated by a cyan circle, while those that form polar interactions are indicated by a magenta circle. Residues invariant across all SPIN homologs and found at the SPIN/rhMPO interface are designated with an orange circle. Note the participation of invariant residues D^{45}, H^{51}, and Y^{75} (per SPIN-*aureus* numbering) in interactions with N^{352} of rhMPO, and how this varies in SPIN-*delphini* by comparing panels C and D above.

Discussion

Though neutrophils serve many essential roles in the innate immune response, the significance of their contributions in preventing bacterial infection is underscored by the manifold strategies *S. aureus* deploys to evade opsonophagocytosis and efficient intracellular killing by these leukocytes [2]. In this regard, the recently identified inhibitor of MPO, SPIN, is one component of a multipartite *S. aureus* evasion program that acts within the maturing phagosome. Although investigations of SPIN-*aureus* have provided vital information on this novel protein [1, 43], the studies we present here are an important step toward a broader understanding of the structure/function relationships of the SPIN protein family. Herein, we have identified eight different SPIN homologs (Fig. 5.1), shown that four homologs bind human MPO (Fig. 5.2), and further demonstrated that three of these can block enzymatic activity of human MPO (Fig. 5.3). We have also determined a 2.4 Å co-crystal structure of SPIN-*delphini* bound to rhMPO (Fig. 5.4), thus allowing the first comparative structural analyses between SPIN proteins in complex with rhMPO (Fig 5.6).

Our work has confirmed that functional SPIN proteins are distributed amongst several bacterial species closely related to *S. aureus*. However, this has also opened up avenues for further investigation. For example, whereas *S. aureus* is a known pathogen of both humans and

livestock (e.g. dairy cattle), several staphylococcal species that encode a SPIN-like sequence (e.g. the *Staphylococcus intemedius* group [80]) are primarily veterinary pathogens. We have previously shown that SPIN-*aureus* exhibits a pronounced binding selectivity and inhibitory capacity toward MPO from known hosts of this organism [1]; this feature is perhaps best illustrated by tight binding to and inhibition of human MPO by SPIN-*aureus*, but an apparent lack of interaction with or inhibition of murine MPO [1]. Consequently, it seems reasonable that several of the SPIN homologs that failed to bind or inhibit human MPO (Fig. 5.2-5.3) might instead display a similar selectivity for MPO proteins derived from their preferred hosts. While additional studies will be necessary to determine whether or not this is the case, an experimental approach similar to those we employed here would be well-suited to addressing this issue.

Separately, our comparative analysis of the SPIN-*aureus*/rhMPO and SPIN-*delphini*/rhMPO complexes has allowed for a more thorough understanding of SPIN/MPO interactions at the sequence/structure level. First, we found no substantially greater level of conservation of the residues at the SPIN/MPO interface (i.e. 17/30 or 17/31 = ~56%) when compared to the two proteins overall (53%) (Figs. 5.4, 5.6 and Table 5.1). This result was somewhat surprising, given that SPIN-*delphini* still maintains a relatively robust interaction with human MPO (K_D = 310 nM) (Fig. 5.2 and Table 5.2). Second, and along these lines, we noted that the numerous changes in SPIN-*delphini* when compared to SPIN-*aureus* manifest themselves as a notably lower overall surface complementary for rhMPO and buried surface area within the SPIN-*delphini*/rhMPO complex. This is particularly true within the α-helical bundle region of the SPIN protein, which drives interaction with MPO [43]. Though it is difficult to infer or test experimentally which of these subtle changes was most detrimental to a highly optimized and cooperative system like a protein/protein interaction, we believe that the

cumulative effects of these alterations must have impacted the observed affinity of the complexes (Fig. 5.2 and Table 5.2).

Finally, we found that the SPIN-*delphini*/rhMPO interface contains a significantly smaller number of polar interactions than does SPIN-*aureus*/rhMPO (Fig. 5.6 and Table 5.4). While some of the differences are due to loss of specific sidechains (e.g. SPIN-*delphini* Q^{74} vs SPIN-*aureus* K^{79}), others are due to unfavorable distances in the SPIN-*delphini*/rhMPO structure as compared to SPIN-*aureus*/rhMPO (e.g. SPIN-*delphini* D^{40} vs SPIN-*aureus* D^{45}). It seems then that changes in both shape complementarity and presentation of key polar groups at the MPO interface are contributing factors to the distinct MPO-binding and inhibitory properties of SPIN-*aureus* and SPIN-*delphini*.

SPIN is not the only staphylococcal innate immune evasion protein that shows strong selectivity for a target molecule from a biologically-relevant host of *S. aureus* [1]. Species selectivity has also been described for the *S. aureus* SCIN family of proteins [89], as SCINs block activity of the alternative complement pathway in humans but not mice [89, 90]. The bi-component pore forming leukocidins of *S. aureus* and related staphylococci likewise show strong preference for interaction with cellular receptors from specific species, thereby explaining their differential effects on target leukocytes from various hosts [91]. Unfortunately, our current understanding of this selectivity is limited primarily to qualitative descriptions of binding and function. While these considerations are clearly useful, we believe that there must also be specific structural and bio/physical-chemical features which underlie such marked host selectivity. This is likely to be true for not only *S. aureus* innate immune evasion proteins, but for any molecules involved in pathogen/host interactions in a much broader sense. Considering that multiple SPIN sequences are now available and that quantitative biochemical, functional, and

comparative structural information on these SPINs bound to MPO from various host species can in theory be obtained, we suggest that the SPIN/MPO interaction can be developed into a valuable model system for understanding the structure/function principles that underlie host specific evolution of virulence proteins.

Chapter 6 - Conclusions and Future Directions

The work described in this dissertation is focused on characterizing a new class of inhibitors that act against the major neutrophil granules component, myeloperoxidase (MPO). While it is well established that neutrophils are essential for our innate defenses, neutrophil-driven inflammation outside this beneficial context lies at the heart of many non-infectious human diseases. The ability to control self-damaging consequences of our immune system requires further understanding of inflammation-triggering enzymes, such as MPO. Studying these enzymes in the context of host-pathogen interaction can lead to the development of new strategies for prevention and treatment of significant human diseases.

S. aureus showed resistance to killing following uptake into the phagosome, which suggests that the bacterium can actively evade specific intracellular killing mechanisms used by neutrophils. SPIN-*aureus* has been showed to play an important role in bacterial survival as it can successfully inhibit human MPO activity [1].

The structure of SPIN was solved using solution NMR for the free form of the protein and x-ray crystallography for SPIN in complex with MPO. We found that SPIN in free (unbound) form has a dynamic N-terminus which changes conformation upon binding to MPO and adopts a β-hairpin confirmation. This N-terminal β-hairpin region of SPIN inserts into the MPO active site, blocking the access of substrate.

Two types of SPIN proteins, deletion mutants and SPIN proteins originating from divergent staphylococcal species, were examined using structural methods, direct binding assays,

and functional assays for MPO activity. These studies allowed us to identify the key residues required for SPIN to maintain its function.

From direct binding assays of SPIN to MPO, we found that SPIN deletion mutants did not have a significant change in their K_D values. However, they lost their ability to inhibit MPO. When examining the SPIN proteins of different staphylococcal origin, we found that SPIN from three species had maintained some degree of binding and function conservation of SPIN-*aureus.* Out of eight species, SPIN originating from *S. delphini* although sharing only ~53% identity to SPIN-*aureus,* retained a strong affinity and inhibitory capacity for human MPO. A 2.4 Å crystal structure of SPIN-*delphini* bound to human MPO provided a basis for comparing the similarities and differences between SPIN-*aureus* and SPIN-*delphini*.

Overall, the experiments described in this manuscript shed light on the molecular features which determine the specificity of SPIN proteins for MPO and open the path toward the design of synthetic MPO inhibitors.

Although this goal is still far from reach, there are several future experiments that can be envisioned based on the current progress of this work.

One such case would be to continue the recombinant expression and characterization of other SPIN orthologs, where non-staphylococcal pathogens could be included. An example for the study is the SPIN-like protein originating from *Macrococcus canis,* which shares ~59% identity with SPIN-*aureus*. These studies could provide important clues from the evolutionary point of view, vital in identifying the specific residues required for SPIN function which is linked to the pathogen adaptation for a specific host.

Once new SPIN orthologs that inhibit human MPO are identified, a new set of mutations can be made to narrow down the residues responsible for loss/gain of function of these ortholog proteins.

Another approach toward creating an artificial SPIN-like protein would be to design a protein sequence based on the conserved SPIN residues across different staphylococcal species, specifically, from the consensus sequence. This experiment will test if artificial sequences based on SPIN template can be designed and if they can be recombinantly expressed. Since the SPIN sequence identity is highly conserved across species, this artificial protein would be a hybrid adaptable to several different species and should retain some function as MPO inhibitor.

The work on characterizing these different inhibitors was focused on human MPO as a target, but each of the different staphylococcal species has evolved and adapted to a specific host. Measuring the binding affinity and performing functional assays for MPO originating from different species could offer insights on the adaptation of the staphylococcal (and not only) pathogens to different hosts. Zoonotic diseases are very common, and they can be caused by over 60% of the known pathogens. Since the aspects of the innate immune system don't undergo dramatic evolutionary changes, it is very easy for some pathogens to pass from one host to another. This approach could be used to address a similar question based on the similarity to MPO. Would SPIN be able to inhibit the activity of other peroxidases, such as the eosinophil peroxidase (EPO)?

References

1. de Jong, N.W.M., et al., *Immune Evasion by a Staphylococcal Inhibitor of Myeloperoxidase.* Proc. Natl. Acad. Sci., 2017. **114**: p. 9439-9444.
2. Spaan, A., Surewaard, BGJ, Nijland, R, and van Strijp, JAG, *Neutrophils versus Staphylococcus aureus: a Biological Tug of War.* Annu. Rev. Microbiol., 2013. **67**: p. 629-650.
3. Nauseef, W.M., *How human neutrophils kill and degrade microbes: an integrated view. .* Immunological Reviews, 2007. **219**: p. 88–102.
4. Nauseef, W.M. and N. Borregaard, *Neutrophils at work.* Nat Immunol, 2014. **15**(7): p. 602-611.
5. Faurschou, M. and N. Borregaard, *Neutrophil granules and secretory vesicles in inflammation.* Microbes and Infection, 2003. **5**(14): p. 1317-1327.
6. Amulic, B., et al., *Neutrophil Function: From Mechanisms to Disease.* Annual Review of Immunology, 2012. **30**(1): p. 459-489.
7. Nauseef, W.M., *Myeloperoxidase in human neutrophil host defense.* Cellular microbiology, 2014. **16**(8): p. 1146-1155.
8. Winterbourn, C.C., Hampton, M. B., Livesey, J. H., and Kettle, A. J., *Modeling the Reactions of Superoxide and Myeloperoxidase in the Neutrophil Phagosome.* J. Biol. Chem., 2006. **281**: p. 39860-39869.
9. Korkmaz, B., et al., *Neutrophil Elastase, Proteinase 3, and Cathepsin G as Therapeutic Targets in Human Disease.* Pharmacol. Rev., 2010. **62**: p. 726-759.
10. Pham, C.T.N., *Neutrophil Serine Proteases: Specific Regulators of Inflammation.* Nat. Rev. Immunol., 2006. **6**: p. 541-550.
11. Stapels, D.A., B.V. Geisbrecht, and S.H. Rooijakkers, *Neutrophil Serine Proteases in Antibacterial Defense.* Curr. Opin. Microbiol., 2015. **23C**: p. 42-48.
12. Odeberg, H. and I. Olsson, *Microbicidal Mechanisms of Human Granulocytes: Synergisitc Effects of Granulocyte Elastase and Myeloperoxidase or Chymotrypsin-Like Cationic Protein.* Infect. Immun., 1976. **14**: p. 1276-1283.
13. Odeberg, H., and Olsson, I., *MicrobicidalMechanisms of Human Granulocytes: Synergisitc Effects of Granulocyte Elastase and Myeloperoxidase or Chymotrypsin-Like Cationic Protein. .* Infect. Immun., 1976. **14**: p. 1276-1283.
14. Bone, R., *Gram-positive organisms and sepsis.* Arch Intern Med., 1994. **10**: p. 26-34.
15. Thwaites, G.E., Gant, V., *Are bloodstream leukocytes Trojan Horses for the metastasis of Staphylococcus aureus?* Nat Rev Microbiol 2011. **9**: p. 215–222.
16. Musher DM, L.N., Darouiche RO, Young EJ, Hamill RJ, Landon GC., *The current spectrum of Staphylococcus aureus infection in a tertiary care hospital.* Medicine (Baltimore), 1994. **73**: p. 186-208.

17. Garcia, B.L., Zwarthoff, S. A., Rooijakkers, S. H.M., and Geisbrecht, B. V., *Novel Evasion Mechanisms of the Classical Complement Pathway.* J. Immunol., 2016. **197**: p. 2051-2060.
18. Kim, H.K., Thammavongsa, V., Schneewind, O., and Missiakas, D., *Recurrent Infections and Immune Evasion Strategies of Staphylococcus aureus. .* Curr. Opin. Microbiol. , 2012. **15**: p. 92-99.
19. Lambris, J.D., Ricklin, D., and Geisbrecht, B. V., *Complement Evasion by Human Pathogens. .* Nat. Rev. Microbiol. , 2008. **6**: p. 132-142.
20. Williams, R.J., et al., *Identification of a Novel Gene Cluster Encoding Staphylococcal Exotoxin-Like Proteins: Characterization of the Prototypic Gene and Its Protein Product, SET1.* Infection and Immunity, 2000. **68**(8): p. 4407-4415.
21. Fitzgerald, J.R., et al., *Genome Diversification in Staphylococcus aureus: Molecular Evolution of a Highly Variable Chromosomal Region Encoding the Staphylococcal Exotoxin-Like Family of Proteins.* Infection and Immunity, 2003. **71**(5): p. 2827-2838.
22. Vickery L. Arcus, R.L., Thomas Proft, John D. Fraser and Edward N. Baker, *The Three-dimensional Structure of a Superantigen-like Protein, SET3, from a Pathogenicity Island of the Staphylococcus aureus Genome.* J. Biol. Chem., 2002. **277**: p. 32274-32281.
23. Peschel, A. and M. Otto, *Phenol-soluble modulins and staphylococcal infection.* Nature reviews. Microbiology, 2013. **11**(10): p. 667-673.
24. de Haas, C.J.C., et al., *Chemotaxis Inhibitory Protein of Staphylococcus aureus, a Bacterial Antiinflammatory Agent.* The Journal of Experimental Medicine, 2004. **199**(5): p. 687-695.
25. Prat, C., et al., *A New Staphylococcal Anti-Inflammatory Protein That Antagonizes the Formyl Peptide Receptor-Like 1.* The Journal of Immunology, 2006. **177**(11): p. 8017.
26. Stapels, D.A., et al., *Staphylococcus aureus secretes a unique class of neutrophil serine protease inhibitors. .* Proc Natl Acad Sci, 2014. **111**: p. 13187-92.
27. Bera, A., et al., *Why are pathogenic staphylococci so lysozyme resistant? The peptidoglycan O-acetyltransferase OatA is the major determinant for lysozyme resistance of Staphylococcus aureus.* Molecular Microbiology, 2004. **55**(3): p. 778-787.
28. Ernst Christoph, M. and A. Peschel, *Broad-spectrum antimicrobial peptide resistance by MprF-mediated aminoacylation and flipping of phospholipids.* Molecular Microbiology, 2011. **80**(2): p. 290-299.
29. Pelz A, W.K., Putzbach K, Hentschel P, Albert K, Götz F., *Structure and biosynthesis of staphyloxanthin from Staphylococcus aureus.* J Biol Chem., 2005. **280**: p. 32493-8.
30. Karavolos, M.H., et al., *Role and regulation of the superoxide dismutases of Staphylococcus aureus.* Microbiology, 2003. **149**(10): p. 2749-2758.
31. Cosgrove, K., et al., *Catalase (KatA) and alkyl hydroperoxide reductase (AhpC) have compensatory roles in peroxide stress resistance and are required for survival, persistence, and nasal colonization in Staphylococcus aureus. .* J Bacteriol, 2007. **189**: p. 1025–1035.
32. Fevre, C., Bestebroer, J., Mebius, M. M., De Haas, C. J., van Strijp, J. A. G., Fitzgerald, J. R., and Haas, P.-J. A., *Staphylococcus aureus Proteins SSL6 and SEIX Interact with Neutrophil Receptors as Identified Using Secretome Phage Display. .* Cell. Microbiol., 2014. **16**: p. 1646-1665.
33. Schultz, J., and Kaminker, K., *Myeloperoxidase of the Leucocyte of Normal Human Blood. I. Content and Localization. .* Arch. Biochem. Biophys., 1962. **96**: p. 465-467.

34. Stothard, P., *The Sequence Manipulation Suite: JavaScript programs for analyzing and formatting protein and DNA sequences.* . Biotechniques, 2000. **28**: p. 1102-1104.
35. Geisbrecht, B.V., S. Bouyain, and M. Pop, *An Optimized System for the Expression and Purification of Secreted Bacterial Proteins.* Prot. Expr. Purif., 2006. **46**: p. 23-32.
36. de Jong, N.W.M., et al., *A Structurally Dynamic N-terminal Region Drives Function of the Staphylococcal Peroxidase Inhibitor (SPIN).* Journal of Biological Chemistry, 2018.
37. Barta, M.L., et al., *Crystal structures of Staphylococcus epidermidis mevalonate diphosphate decarboxylase bound to inhibitory analogs reveal new insight into substrate binding and catalysis.* J. Biol. Chem., 2011. **286**: p. 23900-23910.
38. Woehl, J., Takahashi, D, Herrera, AI, Geisbrecht, BV, Prakash, O *1H, 15N, and 13C resonance assignments of Staphylococcus aureus extracellular adherence protein domain 4.* Biomol NMR Assign, 2016. **10**: p. 301-5.
39. Nauseef, W.M., *Isolation of Human Neutrophils from Venous Blood.* Methods Mol. Biol. , 2014. **1124**: p. 13-18.
40. Schwartz, J., Leidal, K. G., Femling, J. K., Weiss, J. P., and Nauseef, W. M., *Neutrophil Bleaching of GFP-expressing Staphylococci: Probing the Intraphagosomal Fate of Individual Bacteria.* . J. Immunol., 2009. **183**: p. 2632-2641.
41. Greenlee-Wacker, M.C., Rigby, K. M., Kobayashi, S. D., Porter, A. R., Deleo, F. R., and Nauseef, W. M., *Phagocytosis of Staphylococcus aureus by Human Neutrophils Prevents Efferocytosis and Induces Programmed Necrosis.* . J. Immunol., 2014. **192**: p. 4709-4717.
42. Otwinowski, Z., Minor, W., *Processing of X-ray Diffraction Data Collected in Oscillation Mode.* Methods Enzymol., 1997. **276**: p. 307-326.
43. de Jong, N.W.M., et al., *A Structurally Dynamic N-terminal Region Drives Function of the Staphylococcal Peroxidase Inhibitor (SPIN).* J. Biol. Chem., 2017: p. IN PRESS.
44. A.J. McCoy, R.W.G.-K., P.D. Adams, M.D. Winn, L.C. Storoni, R.J. Read, *Phaser Crystallographic Software.* J. Appl. Cryst., 2007. **40**: p. 658-674.
45. P.D. Adams, R.W.G.-K., L.-W. Hung, T.R. Ioerger, A.J. McCoy, N.W. Moriarty, R.J. Read, J.C. Sacchettini, N.K. Sauter, T.C. Terwilliger, *PHENIX: Building New Software for Automated Crystallographic Structure Determination.* Acta Cryst., 2002. **D58**: p. 1948-1954.
46. Adams, P.D., et al., *PHENIX: a comprehensive Python-based system for macromolecular structure solution.* Acta Cryst. , 2010. **D66**: p. 213-221.
47. Farrow, N.A., et al., *Backbone Dynamics of a Free and a Phosphopeptide-Complexed Src Homology 2 Domain Studied by 15N NMR Relaxation.* Biochemistry, 1994. **33**(19): p. 5984-6003.
48. Kay, L.E., et al., *Pulse sequences for removal of the effects of cross correlation between dipolar and chemical-shift anisotropy relaxation mechanisms on the measurement of heteronuclear T1 and T2 values in proteins.* Journal of Magnetic Resonance (1969), 1992. **97**(2): p. 359-375.
49. Johnson, B.A., and Blevins, R. A., *NMRView: A computer program for the visualization and analysis ofNMRdata.* J. Biomol.NMR, 1994. **4**: p. 603–614.
50. Delaglio, F., Grzesiek, S, Vuister, GW, Zhu, G, Pfeifer, J and Bax, A *NMRPipe: a multidimensional spectral processing system based on UNIX pipes.* . J. Biomol. NMR, 1995. **6**: p. 277-293.

51. Keller, R., *The Computer Aided Resonance Assignment Tutorial* ISBN 3-85600-112-3, 2004.
52. Ploscariu, N.T., Herrera, A. I., Jayanthi, S., Kumar, T. K. S., Geisbrecht, B. V., and Prakash, O., *Backbone and Side-Chain 1H, 15N, and 13C Resonance Assignments of a Novel Staphylococcal Inhibitor of Myeloperoxidase.* Biomol. NMR Assign., 2017. **11**: p. 285-288.
53. Shen, Y.a.B., A. , *Protein backbone and sidechain torsion angles predicted from NMR chemical shifts using artificial neural networks.* . J. Biomol. NMR, 2013. **56**: p. 227-241.
54. Lange, O.F., Rossi, P., Sgourakis, N. G., Song, Y., Lee, H.-W., Aramini, J. M., Ertekin, A., Xiao, R., Acton, T. B., Montelione, G. T., and Baker, D., *Determination of solution structures of protein up to 40 kDa using CS-rosetta with sparse NMR data from deuterated samples.* Proc. Natl. Acad. Sci. U.S.A., 2012. **109**: p. 10873–10878.
55. Shen, Y., et al., *De novo structure generation using chemical shifts for proteins with high-sequence identity but different folds.* Protein Science, 2010. **19**(2): p. 349-356.
56. Lowy, F.D., *Staphylococcus Aureus Infections.* The New England Journal of Medicine, 1998. **339**: p. 520-32.
57. Archer, G.L., *Staphylococcus aureus: a well-armed pathogen.* Clin Infect Dis, 1998. **26**: p. 1179-1181.
58. Foster, T., *Immune evasion by staphylococci.* Nature Reviews Microbiology, 2005. **3**: p. 948-958.
59. Kruger, P., Saffarzadeh, M, Weber ANR, Rieber, N, Radsak, M, von Bernuth, H, Benarafa, C, Roos, D, Skokowa J, Harti, D, *Neutrophils: Between host defence, immune modulation, and tissue injury.* . Plos Pathogens, 2015. **11**: p. e1004651.
60. Kolaczkowska, E.a.K., P, *Neutrophil recruitment and function in health and inflammation.* Nat Rev Immunol., 2013. **13**: p. 159-75.
61. Shacter, E.a.W., SA, *Chronic Inflammation and Cancer.* Oncology, 2002. **16**: p. 217.
62. Kleckner, I.R., and Foster, M. P., *An Introduction to NMR-Based Approaches for Measuring Protein Dynamics.* . Biochim. Biophys. Acta, 2011. **1814**: p. 942-968.
63. Wishart, D.S., Sykes, B. D., and Richards, F. M., *Relationship Between Nuclear Magentic Resonance Chemical Shift and Protein Secondary Structure.* . J. Mol. Biol. , 1991. **222**: p. 311-333.
64. Krissinel, E. and K. Henrick, *Inference of macromolecular assemblies from crystalline state.* J Mol Biol, 2007. **372**(3): p. 774-97.
65. Denys, G.A., Grover, P., O'Hanley, P., and Stephens, J. T. J., *In vitro Antibacterial Activity of E-101 Solution, a Novel Myeloperoxidase-Mediated Antimicrobial, Against Gram-Positive and Gram-Negative Pathogens.* J. Antimicrob. Chemother., 2011. **66**: p. 335-342.
66. Stapels, D.A., Geisbrecht, B. V., and Rooijakkers, S. H., *Neutrophil Serine Proteases in Antibacterial Defense.* . Curr. Opin. Microbiol., 2015. **23C**: p. 42-48.
67. Reeves, E.P., Lu, H., Jacobs, H. L., Messina, C. G., Bolsover, S., Gabella, G., Potma, E. O., Warley, A., Roes, J., and Segal, A.W. , *Killing Activity of Neutrophils is Mediated Through Activation of Proteases by K+ Flux.* Nature, 2002. **416**: p. 291-297.
68. Campbell, E.J., Campbell, M. A., and Owen, C. A., *Bioactive Proteinase 3 on the Cell Surface of Human Neutrophils: Quantification, Catalytic Activity, and Susceptibility to Inhibition.* J. Immunol., 2000. **165**: p. 3366-3374.

69. Campbell, E.J., Silverman, E. K., and Campbell,M. A., *Elastase and Cathepsin G of Human Monocytes. Quantificaiton of Cellular Content, Release in Response to Stimuli, and Heterogeneity in Elastase-Mediated Proteolytic Activity.* J. Immunol. , 1989. **143**: p. 2961-2968.
70. Korkmaz, B., Horwitz,M. S., Jenne, D. E., and Gauthier, F., *Neutrophil Elastase, Proteinase 3, and Cathepsin G as Therapeutic Targets in Human Disease.* Pharmacol. Rev., 2010. **62**: p. 726-759.
71. Palazzolo-Ballance, A.M., Reniere, M. L., Braughton, K. R., Sturdevant, D. E., Otto, M., Kreiswirth, B. N., Skaar, E. P., and Deleo, F. R., *NeutrophilMicrobicides Induce a Pathogen Survival Response in Community-Associated Methicillin-Resistant Staphylococcus aureus.* . J. Immunol. , 2008. **180**: p. 500-509.
72. Stapels, D.A.C., et al., *Staphylococcus aureus Secretes a Novel Class of Neutrophil-Serine-Protease Inhibitors that Promote Bacterial Infection.* Proc. Natl. Acad. Sci. U.S.A., 2014. **111**: p. 13187-13192.
73. Chapman, A.L., Mocatta, T. J., Shiva, S., Seidel, A., Chen, B., Khalilova, I., Paumann-Page, M. E., Jameson, G. N., Winterbourn, C. C., and Kettle, A. J., *Ceruloplasmin is an Endogenous Inhibitor of Myeloperoxidase.* J. Biol. Chem., 2013. **288**: p. 6465-6477.
74. Stapels, D.A., Kuipers, A., von Koeckritz-Blickwede, M., Ruyken, M., Tromp, A. T., Horsburgh, M. J., de Haas, C. J., van Strijp, J. A., van Kessel, K. P., and Rooijakkers, S. H., *Staphylococcus aureus Protects its Immune-Evasion Proteins Against Degradation by Neutrophil Serine Proteases.* Cell Microbiol., 2016. **18**: p. 536-545.
75. Nielsen, H., *Predicting Secretory Proteins with SignalP*, in *Protein Function Prediction*, D. Kihara, Editor. 2017. p. 59-73.
76. Sievers F., W.A., Dineen D.G., Gibson T.J., Karplus K., Li W., Lopez R., McWilliam H., Remmert M., Söding J., Thompson J.D., Higgins D., *Fast, scalable generation of high-quality protein multiple sequence alignments using Clustal Omega.* Mol Syst Biol., 2011. **7**.
77. Corpet, F., *Multiple sequence alignment with hierarchical clustering.* Nucl. Acids Res., 1988. **16**: p. 10881-10890.
78. Lamers, R.P., et al., *Phylogenetic relationships among Staphylococcus species and refinement of cluster groups based on multilocus data.* BMC Evolutionary Biology, 2012. **12**: p. 171.
79. Taponen S, S.K., Piessens V, Van Coillie E, De Vliegher S, Koort JM. , *Staphylococcus agnetis sp. nov., a coagulase-variable species from bovine subclinical and mild clinical mastitis.* Int J Syst Evol Microbiol, 2012. **62**: p. 61-65.
80. Sasaki, T., et al., *Reclassification of Phenotypically Identified Staphylococcus intermedius Strains.* J. Clin. Microbiol., 2007. **45**: p. 2770-2778.
81. Stepanovic, S., et al., *Identification and Characterization of Clinical Isolates of Members of the Staphylococcus sciuri Group.* J. Clin. Microbiol., 2005. **43**: p. 956-958.
82. Kloos, W.E., K.H. Schleifer, and R.F. Smith, *Characterization of Staphylococcus sciuri sp. nov. and Its Subspecies.* Int. J. Syst. Bact., 1976. **26**: p. 22-37.
83. Robert, X. and P. Gouet, *Deciphering Key Features in Protein Structures with the New ENDscript Server.* Nucleic Acids Res., 2014. **42(W1)**: p. W320-W324.
84. de Jong, N.W.M., et al., *Immune Evasion by a Staphylococal Inhibitor of Myeloperoxidase.* Proc. Natl. Acad. Sci. U.S.A., 2017. **114**: p. 9439-9444.

85. Fiedler, T.J., C.A. Davey, and R.E. Fenna, *X-ray Crystal Structure and Characterization of Halide-Binding Sites of Human Myeloperoxidase at 1.8 A Resolution.* J. Biol. Chem., 2000. **275**: p. 11964-11971.
86. Zeng, J. and R.E. Fenna, *X-ray Crystal Structure of Canine Myeloperoxidase at 3 A Resolution.* J. Mol. Biol., 1992. **226**: p. 185-207.
87. Shrake, A. and J.A. Rupley, *Environment and Exposure to Solvent of Protein Atoms.* J. Mol.Biol. , 1997. **79**: p. 351-371.
88. Lawrence, M.C. and P.M. Colman, *Shape Complementarity at Protein/Protein Interfaces.* J. Mol. Biol., 1993. **234**: p. 946-950.
89. Rooijakkers, S.H., et al., *Immune Evasion by a Staphylococcal Complement Inhibitor that Acts on C3 Convertases.* Nat. Immunol., 2005. **6**: p. 920-927.
90. Jongerius, I., et al., *Staphylococcal Complement Evasion by Various Convertase-blocking Molecules* J. Exp. Med., 2007. **204**: p. 2461-2471.
91. Spaan, A.N., J.A.G. van Strijp, and V.J. Torres, *Leukocidins: Staphylococcal Bi-Component Pore-Forming Toxins Find Their Receptors.* Nat. Rev. Microbiol., 2017. **15**: p. 435-447.